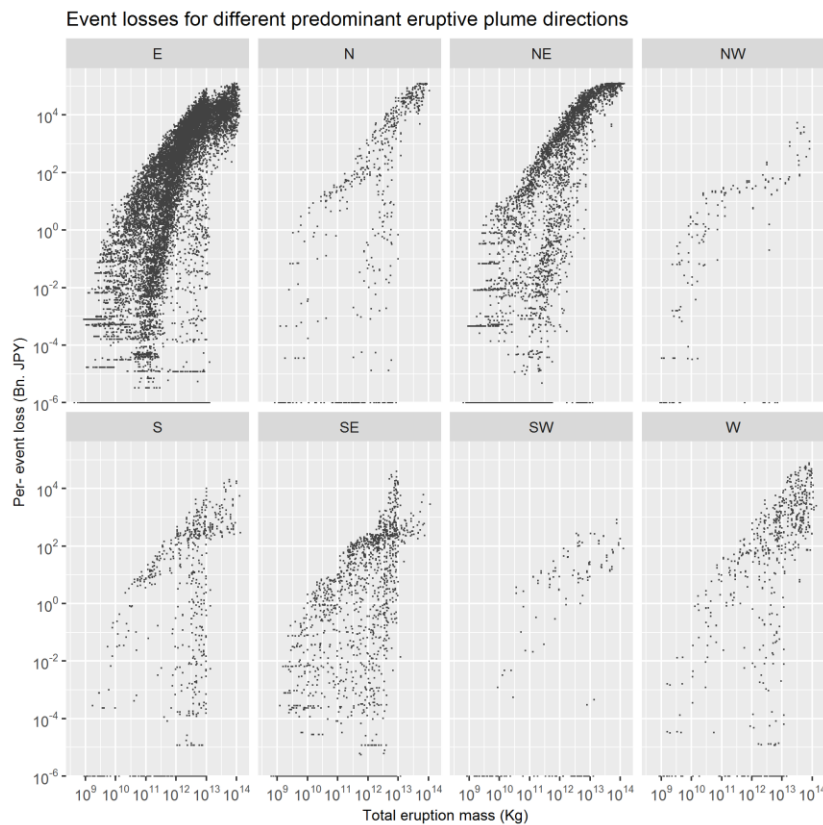


1 Author's Response

2 Reviewer #1:

3 1. I am surprised that total eruption mass is not found to be a sensitive indicator of loss and does not appear in
4 the parametric trigger design. Obviously, for explosive eruptions there is some correlation between eruption
5 column height and loss, but not necessarily. For example, the Eyjall (Iceland) eruption mentioned in the intro did
6 not have a particularly high plume, yet caused loss (although not for buildings – the focus of this paper). Does
7 the point cloud shown in figure 3 collapse significantly (or is it significantly different) for eruption mass rather than
8 plume height?
9

10 **Authors:** We have produced a graph equivalent to that of Figure 3 of the manuscript, showing the relationship
11 between total eruption mass and modelled loss (please see below). Comparison between this Figure and Figure
12 3 shows that eruption mass is, as rightly pointed out by the reviewer, a sensible indicator of loss. The reason that
13 eruption mass does not appear in the parametric design, however, is because it does not fulfill the requisite of
14 being obtainable on a near-real time basis (condition number 2 in Section 3) - even though it does fulfill conditions
15 1 and 3 mentioned in the Section. Whereas eruption column height is readily observable and can be objectively
16 measured and reported on a real-time basis (as currently done by JMA), measurement/ estimation of eruption
17 mass is not currently performed and reported on a real time basis. The parametric design, on the other hand and
18 by definition, expects a non-perfect-relationship between the value of the chosen physical parameter and the
19 resulting loss, which is incorporated in the basis risk (Section 3.2).
20



21 2. Similarly, eruption duration has a significant impact on loss and might be a useful part of the parametric trigger
22 design. Unlike earthquakes, volcanic eruptions may have significant duration (years). The eruption duration not
23 only impacts total load (and the ability to remove the load) but also the sectors (N,NE, etc.) likely to be impacted
24 by the eruptions. Some mention of variable duration and its complicated influence on risk is warranted.
25
26
27

28 **Authors:** This is a very important observation and indeed the duration of the eruption should prove a significant
29 driver of the loss. The reason why it wasn't included in the parametric design, however, is because it does not
30 fulfill condition number 3 in Section 3 (eruption duration is not part of the stochastic event set in the catastrophe
31 risk model developed). In this case, indeed, it is not possible to show the relationship between loss and eruption
32 duration because the data is not available (contrary to the earlier case of loss versus eruption mass), although
33 on the other hand a degree of correlation between eruption duration and total eruption mass is expected. Future
34 development of more complex and complete eruption catastrophe risk models should enable further investigation
35 of alternative parametric designs for volcanic eruptions, using different –or a combination of different- triggers.
36 We believe it is important however to discuss these issues in the current paper and have added comment in this
37 respect (line 312+ of pdf Manuscript).

38
39
40 3. Plume height is measured remotely by satellite, and so fulfills a requirement of parametric trigger design to be
41 quickly calculated and unbiased, compared with eruption mass. I think you should cite some important literature
42 on this, like:

43
44 Prata, A.J. and Grant, I.F., 2001. Retrieval of microphysical and morphological properties of volcanic ash plumes
45 from satellite data: Application to Mt Ruapehu, New Zealand. Quarterly Journal of the Royal Meteorological
46 Society, 127(576), pp.2153- 2179.

47
48 Pardini, F., Burton, M., Arzilli, F., La Spina, G. and Polacci, M., 2018. SO₂ emissions, plume heights and
49 magmatic processes inferred from satellite data: The 2015 Calbuco eruptions. Journal of Volcanology and
50 Geothermal Research, 361, pp.12-24. Merucci, L., Zakšek, K., Carboni, E. and Corradini, S., 2016. Stereoscopic
51 estimation of volcanic ash cloud-top height from two geostationary satellites. Remote Sensing,
52 8(3), p.206.

53
54 **Authors:** Thank you very much for pointing this work out and have included (line 535 of pdf Manuscript).

55
56
57 4. One of the authors, C. Magill, has an important paper on tephra modeling in the Toyko region using Tephra2
58 to forecast loss. It is important to cite that paper because it provides essential groundwork for using Tephra2
59 to make these models, which is not covered in the current manuscript, whereas the current manuscript goes much
60 farther in terms of illustrating a workflow for designing the parametric trigger. Magill, C., Mannen, K., Connor, L.,
61 Bonadonna, C. and Connor, C., 2015. Simulating a multi-phase tephra fall event: inversion modelling for the
62 1707 Hiei eruption of Mount Fuji, Japan. Bulletin of Volcanology, 77(9), p.81.

63
64 **Authors:** Absolutely- it makes sense including this reference (line 169 of pdf Manuscript).

65
66
67 5. In addition to VEI, you might mention alternative eruption scales, like magnitude. See:

68
69 Pyle, D.M., 2015. Sizes of volcanic eruptions. In The encyclopedia of volcanoes (pp. 257-264). Academic Press.
70 Rougier, J., Sparks, R.S.J., Cashman, K.V. and Brown, S.K., 2018. The global magnitude–frequency relationship
71 for large explosive volcanic eruptions. Earth and Planetary Science Letters, 482, pp.621-629.

72
73 **Authors:** Thank you for pointing this out and have included (footnote #1 of pdf Manuscript)

74
75
76 6. Just a few detailed comments:

77
78 • Change Kg to kg (lower case). Elsewhere in the paper, some units are capitalized. They should always
79 be lower case.

80
81 **Authors:** thanks for pointing out, changes made throughout text

82
83 • Instead of saying vertical wind speed, say variation in wind speed with height in the atmosphere.

84

85 **Authors:** the original sentence (“The model takes into account appropriate vertical wind speed and
86 direction profiles”) is not clear, we referred to “vertical profiles of both wind speed and direction”. We can
87 have re-written in line 170 of pdf Manuscript.
88

- 89 • Around line 293 – what is the relationship of eruption column height with total mass and eruption
90 duration?
91

92 **Authors:** We have included commentary on this relationship, as per discussion following from reviewer’s
93 comments 1 and 2 (line 312+ of pdf Manuscript).
94

- 95 • Around line 510: it seems to me there is a fundamental difference between tephra fallout and these other
96 phenomena (lava flows, pdcs, etc.). Tephra causes variable loading (depending on the eruption
97 magnitude) so it seems more analogous to earthquake damage. The other phenomena cause complete
98 destruction to property in their path. So how does this influence the parametric trigger design? It must
99 be binary for these other phenomena? Wrap this discussion back to the equations you present.
100

101 **Authors:** This is an interesting and thought provoking observation. Whereas tephra fallout can be
102 considered as a gradually varying phenomenon that causes varying levels of damage, volcanic mass
103 flows tend to produce either a total loss (assets in their path) or no loss (assets away from their path).
104 The present work focuses solely on the design of a parametric trigger for tephra fallout, which has
105 adopted the form of a Multilayer trigger in this particular study (Section 3.2). Regarding the potential
106 design of a parametric trigger for volcanic mass flows, this is something that would have to be
107 thoroughly investigated in future work. It may be the case that a Binary trigger (Section 3.2) would be
108 appropriate; however, it is our view that a Multilayer trigger cannot be ruled out in principle, and that
109 the binary nature of the damage/loss does not necessarily warrant the selection of a Binary trigger
110 over a Multilayer trigger. It is our view that the design of a parametric trigger for these volcanic
111 phenomena will substantially be determined by the characteristics of the physical modelling
112 methodology applied.

113 **Reviewer #2:**

- 114 1. Some of the arguments in the introduction should be more clearly supported by evidence from the literature.
115 For example, on line 100-102, provide literature to support the statement about the proper choice of parameters.
116

117 **Authors:** Further background and references on this topic have been provided in line 100+ of pdf Manuscript.
118
119

- 120 2. Wet version: on lines 165-171, the authors describe how they developed the “wet version” of the scenarios.
121 They refer to a paper by Macedonio and Costa (2012) for the approach. Whilst this is fine, a short overview of
122 this methods should also be summarized in this paper to give the reader an overall understanding of how it works
123 (referring the reader to the paper for the details of course).
124

125 **Authors:** Further details have been provided in line 176+ of pdf Manuscript.
126

- 127 3. Vulnerability functions: Figure 2 gives a clear example of two vulnerability curves. However, for reproducibility,
128 have the authors considered providing all curves, for example in a supplementary dataset?
129

130 **Authors:** The source of the damage functions has been specified and referenced in the paper (GAR15 Regional
131 Vulnerability Functions report by Maqsood et al., 2015), which contains a comprehensive Annex with graphs for
132 all the ash fall damage functions by construction type, building rise and roof pitch.
133

- 134 4. BE module: please provide more information on how this is done – for example, how does the assignment on
135 the probabilistic basis work?
136

137 **Authors:** Further details have been provided in line 227+ of pdf Manuscript.
138

139 5. Parts of the current conclusion would better split out into a separate discussion section. In particular, the parts
140 discussing the limitations and challenges, as well as applicability elsewhere. This would give the opportunity to
141 slightly expand these aspects, with reference to key literature. For example, given the topic of the special issue,
142 one of two extra paragraphs describing key challenges for upscaling globally would be useful (there is some
143 reasoning along this line but it is very short). The conclusion could then be kept shorter and more succinct.
144

145 **Authors:** The Conclusions section has been split into Discussion and Conclusions as advised (line 503+ of pdf
146 Manuscript), and these topics have been expanded with the following additional references added:

147
148 Blong R., Tillyard C., Attard G. (2017) Insurance and a Volcanic Crisis—A Tale of One (Big) Eruption, Two
149 Insurers, and Innumerable Insureds. In: Fearnley C.J., Bird D.K., Haynes K., McGuire W.J., Jolly G. (eds)
150 Observing the Volcano World. Advances in Volcanology (An Official Book Series of the International
151 Association of Volcanology and Chemistry of the Earth’s Interior – IAVCEI, Barcelona, Spain). Springer, Cham.
152 https://doi.org/10.1007/11157_2016_42
153

154 Brown, S.K.; Loughlin, S.C.; Sparks, R.S.J.; Vye-Brown, C.; Barclay, J.; Calder, E.; Cottrell, E.; Jolly,
155 G.; Komorowski, J.-C.; Mandeville, C.; et al. Global volcanic hazard and risk. In Global Volcanic Hazards and
156 Risk; Cambridge University Press: Cambridge, UK, 2015; pp. 81–172. ISBN 9781316276273
157

158 Guéhenneux, Y.; Gouhier, M.; Labazuy, P. Improved space borne detection of volcanic ash for real-time
159 monitoring using 3-Band method. J. Volcanol. Geotherm. Res. 2015, 293, 25–45.
160

161 Loughlin, S., Sparks, S., Brown, S., Jenkins, S., & Vye-Brown, C. (Eds.). (2015). Global Volcanic Hazards and
162 Risk. Cambridge: Cambridge University Press. doi:10.1017/CBO9781316276273
163

164 Valade, S.; Ley, A.; Massimetti, F.; D’Hondt, O.; Laiolo, M.; Coppola, D.; Loibl, D.; Hellwich, O.; Walter, T.R.
165 Towards Global Volcano Monitoring Using Multisensor Sentinel Missions and Artificial Intelligence: The MOUNTS
166 Monitoring System. *Remote Sensing*, 2019, 11, 1528.

167

168

169

170

171

172

173

174

175

176

177 **Design of parametric risk transfer solutions for volcanic**
178 **eruptions: an application to Japanese volcanoes**

179 Delioma Oramas-Dorta¹, Giulio Tirabassi¹, Guillermo Franco¹, Christina Magill²

180 ¹ Guy Carpenter & Co, LLC. Tower Place West, London, EC3 5BU, United Kingdom.

181 ² Department of Environmental Sciences, Faculty of Science and Engineering, Macquarie University, NSW 2109,
182 Australia.

183 *Correspondence to:* Dr. Delioma Oramas-Dorta (Delioma.Oramas-Dorta@guycarp.com).

184

185

186

187

188

189

190

191

192

193

194

195

196

197

198

199

200

201

202

203

204 **Abstract**

205 Volcanic eruptions are rare but potentially catastrophic phenomena, affecting societies and economies through
206 different pathways. The 2010 Eyjafjallajökull eruption in Iceland, a medium-sized ash fall producing eruption, caused
207 losses in the range of billions of dollars, mainly to the aviation and tourist industries. Financial risk transfer
208 mechanisms such as insurance are used by individuals, companies, Governments, etc. to protect themselves from
209 losses associated to natural catastrophes. In this work, we conceptualize and design a parametric risk transfer
210 mechanism to offset losses to building structures arising from large, ash fall-producing volcanic eruptions. Such
211 transfer mechanism relies on the objective measurement of physical characteristics of volcanic eruptions that are
212 correlated with the size of resulting losses (in this case, height of the eruptive column and predominant direction of
213 ash dispersal), in order to pre-determine payments to the risk cedant concerned. We apply this risk transfer mechanism
214 to the case of Mount Fuji in Japan, by considering a potential risk cedant such as a regional Government interested in
215 offsetting losses to dwellings in the heavily populated Prefectures of Tokyo and Kanagawa. The simplicity in
216 determining eruptive column height and ash fall dispersal direction makes this design suitable for extrapolation to
217 other volcanic settings world-wide where significant ash fall producing eruptions may occur, provided these
218 parameters are reported by an official, reputable agency, and a suitable loss model is available for the volcanoes of
219 interest.

220

221

222

223

224

225

226

227

228

229

230

231

232

233

234

235

236

237

238 1 Introduction

239 Volcanic eruptions are complex phenomena that generate a variety of hazards such as lava flows, ash fall, pyroclastic
240 flows, lahars, and volcanic earthquakes. These may in turn cause physical damage to man-made structures and the
241 discontinuation of activities related to aviation, tourism, and agriculture, among others.

242 Although rare, large volcanic eruptions pose significant destructive and disruptive potential. A medium-sized eruption
243 like the 2010 Eyjafjallajökull eruption in Iceland (VEI¹ 4) caused the cancellation of about one hundred thousand
244 flights and carried an estimated global cost of US\$4.7 Billion (Oxford Economics, 2010). According to estimates by
245 the Government of Japan, a repeat of the December 1707 Mt. Fuji eruption (VEI 5) could result in national losses over
246 US\$22.5 Billion (Cabinet Office of Japan, 2002), not including impacts on transportation and power transmission
247 facilities that could effectively paralyze the Tokyo metropolitan area. Mt. Tambora's 1815 eruption in Indonesia (VEI
248 7) is regarded as the greatest eruption in historic time, ejecting as much as 175 km³ of pyroclastic material that reached
249 heights of over 40 km into the atmosphere (Self et al., 1984). It caused an estimated death toll of 71,000 people some
250 of which due to the immediate explosion that killed around 12,000 people on Sumbawa Island (Oppenheimer, 2003).
251 The event triggered tsunami waves striking several Indonesian islands and a famine related to eruptive fallout ruining
252 crops in the region (Stothers, 1984; Oppenheimer, 2003). At present, over one million people live within 100km of
253 Mt. Tambora (GVP, 2019).

254 Insurance is a mechanism to protect against financial losses from natural perils. Through insurance, people and entities
255 transfer risks to insurance companies in return for the payment of an annual premium. These premiums are
256 accumulated in order to build up reserves that enable them to pay claims in case of need. Insurance companies,
257 similarly, can accept only a certain amount of risk, after which they may themselves seek protection through
258 reinsurance. Companies who sell reinsurance are typically global in nature, hedging their risk in one region by selling
259 products in another or by seeking insurance mechanisms themselves for their own portfolios (this is called
260 "retrocession"). Through this chain of risk transfer accumulations of risk are successfully shared among many parties
261 across the world, ideally enabling our society to cope with potentially large losses without any particular entity in this
262 chain suffering unrecoverable losses.

263
264 As concentrations of risks grew, the capital available to supply global reinsurance products was in more demand,
265 which had the consequence of raising prices. A larger supply of capital was necessary and there were large yields
266 available for those interested. This gave rise to the appearance of Insurance Linked Securities (ILS), a type of financial
267 instrument that allowed the capital markets to enter the insurance space in what has been referred to as "the
268 convergence market," thus increasing the amount of capital available for insurance-related operations. One tool that
269 falls into this category is a catastrophe (cat) bond, a means of fragmenting risk into coupon bonds that can be sold to
270 qualified investors (Cummins, 2008; Swiss Re, 2011).

271
272 As new investors in this space lack familiarity with traditional insurance operations, there has been an interest in
273 devising some of these instruments as a form of derivative that simplifies the process of settling a claim (World
274 Economic Forum, 2008). This motivation gave rise to "parametric cat bonds" in which recoveries after a catastrophe
275 event are tied to the occurrence of a set of measurable physical characteristics, such as the magnitude of an earthquake
276 or the category of a hurricane, rather than to actual losses or indemnity. Properly chosen parameters that are easy to
277 measure transparently and with accuracy can provide parametric cat bonds with a speed of payment unparalleled in
278 the domain of insurance. The choice of parameters has evolved since the 1990's when these tools first appeared,

¹ The Volcanic Explosivity Index (VEI) is a relative measure of the explosiveness of volcanic eruptions devised by Chris Newhall and Stephen Self in 1982. The scale is open-ended with the largest eruptions in history given magnitude 8. The scale is logarithmic from VEI 2 upwards, with each interval on the scale representing a tenfold increase in volume of eruptive products. Another measures commonly used for eruption size is eruption Magnitude (e.g. Pyle, 2015).

279 resulting in different choices of design. For instance, in the case of earthquake two types of solutions have been used
280 in the market successfully: first generation CAT-in-a-box triggers, and second-generation parametric indices. The first
281 type is based on the magnitude, epicenter location, and focal depth of the event, whereas the second are based on
282 geographically distributed earthquake parameters such as ground motions. Second-generation indices can be, in
283 general, considered to be superior to first generation triggers owing to a potentially better correlation between the
284 distributed parameters and resulting losses, although the performance ultimately depends on many design
285 considerations. In the case of tsunami losses, for instance, Goda et al. (2019) found the forecasting errors in second-
286 generation indices were slightly inferior that those for first generation triggers. Progressively, as sensors become more
287 ubiquitous and precise, and as technology facilitates communication of measurements, parametric insurance
288 mechanisms are becoming more widespread.

289
290 Earthquake parametric cat bond transactions appeared first in 1997 and grew in number throughout the following
291 years, supported by what were then relatively novel techniques to model earthquake risk in the insurance market
292 (Franco, 2014). Since then, these earthquake solutions have taken many forms depending on the parameters chosen
293 for their design and on whether they are binary (pay or no pay) or “index-based” indicating a payment somewhat
294 correlated with the intensity of the event (Wald and Franco, 2016; 2017). A similar development in the field of volcanic
295 risks has not yet taken place. Only one product exists in the market, offered by Sompo Japan Nipponkoa Insurance
296 that provides coverage on a parametric basis for volcanic eruptions. This product is addressed to commercial
297 corporations in Japan at risk of experiencing losses derived from a volcanic eruption (Artemis, 2016). Tailored in
298 particular to the tourism industry, it grants coverage of losses up to US\$10 million from business interruption caused
299 by the onset of a level 3 or above eruption alert as determined by the Japan Meteorological Agency (JMA) (Yamasato
300 et al., 2013).

301
302 The dearth of insurance derivative products linked to physical characteristics of volcanic eruptions may be partly
303 explained by the lack of fully probabilistic volcano loss models, which are a pre-requisite for the design and calibration
304 of these products. In this paper we present a stochastic volcanic risk model for six Japanese volcanoes on which we
305 base the construction of a parametric risk transfer tool. First, in Sect. 2 we describe the components of the risk model;
306 i.e. hazard, vulnerability, exposure, and loss computation. In Sect. 3, we discuss the conceptualization and the
307 mathematical design of a plausible parametric risk transfer tool leveraging physical descriptors of the eruptive events
308 that are both simulated in the risk model as well as reported by public entities during the course of an actual event.
309 The work draws from efforts carried out in the development of parametric triggers for other perils, fundamentally
310 earthquake (Franco, 2010; Franco, 2013; Goda, 2013; Goda, 2014; Pucciano et al. 2017; Franco et al. 2018) and
311 tsunami (Goda et al. ~~2018~~2019). Sect. 4 applies the framework presented to an application case study in Japan where
312 a regional (or national) entity may desire to adopt this type of risk transfer mechanism to help offset costs associated
313 with ash-fall generated by an eruption of Mt. Fuji. Conclusions and final remarks are collected in Sect. 5 where we
314 elaborate on the potential application of this type of tool in a generalized, volcanic, global setting.

315
316

317 **2 Construction of a volcano risk model**

318 Japan is one of the most volcanically active countries in the world. There are 111 active volcanoes in Japan; on average,
319 a total of 15 volcanic events (including eruptions) occur every year, some of which seriously hinder human life (JMA,
320 2019). Five Japanese cities, Tokyo, Osaka, Nagoya, Sapporo and Fukuoka, are ranked among the top-20 cities most
321 at risk from volcanic eruptions according to the Lloyd’s City Risk Index (Lloyd’s, 2018).

322 The development of a volcanic risk model for Japanese volcanoes allows improving our ability to quantify said risk
323 as a preliminary step to transferring it to the capital markets. The model focuses on physical damage of buildings
324 arising from significant deposition of volcanic ash (tephra). The geographic scope is limited to the highly populated

325 and industrialized Prefectures of Tokyo and Kanagawa, potentially affected by the surrounding six major volcanoes:
326 Fuji, Hakone, Asama, Haruna, Kita-Yatsugatake and Kusatsu-Shirane (see Fig. 1). The model presented does not
327 consider damage to contents, business interruption, or costs associated with ash fall clean up. Neither does it consider
328 other volcanic hazards such as lava flows, pyroclastic density currents, debris flows or avalanches. The model is
329 structured into four modules: hazard, vulnerability, built environment (or exposure), and loss calculation, which are
330 described in more detail in the following subsections.

331 **Figure 1: The geographic domain of the volcano ash fall model presented in this paper includes Tokyo and Kanagawa**
332 **Prefectures in Japan, and the six major volcanoes that can affect them, Fuji, Hakone, Asama, Haruna, Kita-Yatsugatake,**
333 **and Kusatsu-Shirane.**

334

335 2.1 The hazard module

336 The hazard module consists of a collection of 26,807 volcanic ash fall footprints, each of them associated with one of
337 the six modelled volcanoes and with an annual probability of occurrence (see Table 1).

338

339 **Table 1: Number of volcanic ash fall events included in the model (i.e. those ash fall events that impact the model's**
340 **geographical domain of Tokyo and Kanagawa prefectures) and associated annual probabilities of occurrence by volcano.**
341 **Ash fall events originated by these volcanoes that do not impact the model domain have been excluded from the counts.**

342 This original set of footprints was produced by Risk Frontiers in 2017, and was provided specifically for the purpose
343 of building the volcano risk model that we present in this paper, on an exclusive basis. Modelling was performed using
344 *tephra2* numerical model, which simulates the dispersion of ash fall from a volcanic source using mass conservation
345 and advection-diffusion equations (Bonadonna et al., 2005; Connor and Connor, 2006; [Magill et al., 2015](#)). Tephra
346 accumulation is computed for specified locations surrounding a volcano in load units ($\text{kg}\times\text{m}^{-2}$). The model takes
347 into account ~~vertical atmospheric profiles of both wind speed and direction~~appropriate vertical wind speed and
348 direction profiles, which in this case were generated from reanalysis wind data (NCEP-DOE Reanalysis2; NOAA).

349 The interaction of volcanic ash fall with rainfall may lead to an increase in the weight of the earlier due to absorption
350 of water, leading to increased loads and consequently to potentially more severe damages of affected structures. In
351 order to consider the possibility of ash fall – producing eruptions being concurrent to rainfall, “wet” versions of the
352 footprints were produced, respecting the rainfall patterns in the region of interest. The methodology used to create
353 “wet” footprints follows that described by Macedonio and Costa, 2012, whereby deposited ash fall increases its weight
354 up to the point it becomes saturated with rainfall water, assuming a density of 1000 Kg/m^3 and a total porosity of 60%
355 for deposited ash fall from Mt. Fuji. Following Macedonio and Costa, 2012, we assume that all pores and interstices
356 of the deposit are filled with water (water saturation), if enough water is available from a specific rainfall event.
357 Rainfall data were supplied by JBA Risk Management in the form of 10,000 years of simulated daily precipitation
358 that incorporates tropical cyclone and non-tropical cyclone precipitation, and rainfall data were supplied by JBA Risk
359 Management. This was in the form of 10,000 years of simulated daily precipitation that incorporates tropical cyclone
360 and non-tropical cyclone precipitation; derived by JBA as part of their Global Flood Event Set.

361 2.2 The vulnerability module

362 As mentioned prior, the model considers damage to buildings only (residential, commercial or industrial), arising from
363 the vertical loads imposed by tephra on the structures. The level of damage to a specific building depends on the total
364 ash load and on the structural characteristics of the building. For each building type (i.e. a defined combination of
365 construction type, building rise and roof pitch) the model uses a specific vulnerability function that computes the
366 probability of experiencing a certain level of damage (expressed as a damage ratio of cost of repair versus total cost

367 of replacement) for a given physical load value upon that structure. The vulnerability functions were developed on the
368 basis of several studies on the subject (Spence et al., 2005; Maqsood et al., 2014; Jenkins et al., 2014; Jenkins et al.,
369 2015; Blong et al., 2017) for building typologies common in the area (see Table 2). Given the lack of data on roof
370 type for individual structures, the model assumes probabilities of different roof types within the exposure set (low,
371 medium or high pitch) depending on the building occupancy, construction typology and building rise.

372

373

374 **Table 2: Building types common in the Tokyo and Kanagawa Prefectures of Japan, for which specific vulnerability**
375 **functions were developed in the volcano risk model. RC-SRC stands by “Reinforced Concrete – Steel Reinforced Concrete”.**

376

377 Examples of damage functions used in the volcano risk model are provided in Fig. 2 for two contrasting building types (different
378 construction type, building rise and roof pitch).

379

380 **Figure 2: Damage functions for two different building types considered in the volcano risk model (“RC-SRC” stands for**
381 **Reinforced Concrete- Steel Reinforced Concrete; “Med.” stands for Medium); source of these damage functions is Maqsood**
382 **et al., 2014.**

383

384 *2.3 The exposure and the built environment (BE) modules*

385 These two closely-related modules jointly define the characteristics and monetary values of the group of buildings
386 (“portfolio”) for which the model will produce risk metrics.

- 387 1) The exposure module consists of a database structure that allows the user to characterise the portfolio of
388 interest and upload those details to the risk model in a structured manner, to subsequently run it. The main
389 database fields relate to number of buildings and associated values (i.e. building replacement values),
390 geographical location of the buildings (supported geocoding levels include geographical coordinates, 5 and
391 7 digit Postal Codes and Prefecture), occupancy, construction type and building rise.
- 392 2) The BE module is a database that completes the information provided by the user, wherever it is incomplete
393 or not accurate enough. This database represents the built environment across the model geographical
394 domain, specifically, the number, characteristics and spatial distribution of the different building types as
395 described in Table 2. The purpose of this module is two-fold. On one hand it allows defining the likely
396 location of buildings geo-located at resolutions coarser than geographical coordinate, in order to better
397 characterise their relationship with the spatial distribution of the hazard. The BE distributes buildings into a
398 finer spatial resolution on a probabilistic basis, using weights that are specific to each building type. Weights
399 were computed on the basis of information such as land use and land cover type and census data. In the case
400 of our model, data sources included the 2013 Housing and Land Survey (Statistics Bureau, Government of
401 Japan), the 2014 Tokyo Statistical Yearbook (Tokyo Metropolitan Government), Japan E-Stat (Ministry of
402 Land, Infrastructure, Transport and Tourism), etc. The second purpose of the BE is to infer damage-relevant
403 characteristics of buildings (e.g. building rise, construction type, etc.) if this information is not captured in
404 the description of the buildings we want to model. This is again done on a probabilistic basis, depending on
405 the location of the building and any known characteristics (e.g. building occupancy). To illustrate how the
406 BE works, let us take an example of a Residential building in a Postal Code in Kanagawa prefecture. If that
407 is all the information we know about this asset, the BE module will use the weights corresponding to

408 Residential buildings in that postal code to assign a specific location within the postal code and a set of
409 characteristics (construction type, etc.) to this Residential building (please see Table 2 for a list of possible
410 Residential building types). Such assignation is probabilistic in the sense that a distribution of likely locations
411 and characteristics will be generated for each risk, through iterative sampling based on those weights. Such
412 distribution will eventually be propagated to the loss calculation part of the model, in order to produce a final
413 loss distribution for this building.

414

415 2.4 The loss calculation module

416 The loss calculation module or engine estimates the monetary loss associated to each building for the different events
417 that can potentially affect it. This is attained (for each event-building “interaction”) by multiplying the damage ratio
418 prescribed by the corresponding vulnerability function and the replacement value of the building, which needs to be
419 provided by the modeller. The loss calculation module allows reporting losses by building and by event; as well as by
420 event (aggregate event loss).

421 Volcanic loss data are very scarce due to the low frequencies of damaging eruptions. We used a few independent
422 sources to validate modelled losses. These included two studies on damage estimations of a repeat of the 1707 Fuji
423 eruption (Kuge et al., 2016; Cabinet Office of Japan, 2002) that were used to validate modelled losses from severe
424 eruptions. To validate modelled losses from less severe eruptions, we used as a proxy data on insured building losses
425 caused by loading of snow in Toyo and nearby Prefectures in February 2014 (General Insurance Association of Japan,
426 2015). Kuge et al. (2016) modelled losses for industrial buildings (with an assumed value of 1 Billion JPY per
427 building) if there was a repeat of the Fuji 1707 eruption. Estimated individual building losses ranged between 35 and
428 180 Million JPY (K. Kuge, personal communication, 2017). This compares well with our modelled losses between
429 28.6 and 138.4 Million JPY for industrial buildings, under a reconstruction of the Fuji 1707 eruption. Regarding
430 Residential buildings, the reported average building loss value for the February 2014 snowfall event in Japan was 1.2
431 Million JPY (General Insurance Association of Japan, 2015). Assuming a snow density value of 200 kg/m³, we
432 identified ash fall events in the volcano model producing equivalent loads, and calculated an average Residential
433 building loss of 1.7 Million JPY.

434

435 3 Design of a parametric trigger for volcano risk transfer

436 A parametric trigger refers to a specific value or threshold of a physical, measurable characteristic associated to the
437 natural phenomenon in question (e.g. to ash fall-producing volcanic eruptions in this case, or earthquakes, hurricanes,
438 etc.), above which a significant level of damage of exposed assets (e.g. damage to buildings) is likely to occur. When
439 the physical parameter exceeds that threshold for a particular event, it is considered that a risk cedant should receive
440 a payment commensurate to the loss that their portfolio will likely incur as a result of being exposed to the event.

441 Therefore, when designing a parametric risk transfer mechanism, it is crucial to select a physical parameter that
442 correlates well with potential losses. In the case of parametric earthquake risk transfer, for instance, it is common to
443 select the magnitude of the earthquake as the main parameter, and subsequently define threshold value/s for the
444 magnitude scale, above which significant damages are likely to occur (Franco, 2010; Franco, 2013). Other alternatives
445 used in practice consider shaking measurements such as peak ground accelerations or spectral accelerations at a set of
446 locations (Goda, 2013; Goda, 2014; Pucciano et al. 2017).

447 There are three important requirements for the selection of a physical characteristic of a natural phenomenon to be
448 used as a parametric trigger in the design of a risk transfer mechanism:

- 449 1) The parameter must exhibit strong correlation to losses incurred as a consequence of the physical phenomenon.
- 450 2) The parameter needs to be measured and reported by a reliable and impartial organisation on a near-real time
451 basis. In the case of earthquakes, for instance, earthquake information is often obtained from reliable international
452 bodies such as the U.S. Geological Survey (Wald & Franco, 2017).
- 453 3) Finally, each of the stochastic events in the catastrophe risk model used as a basis to design the risk transfer
454 solution must explicitly include the corresponding value for the selected physical parameter. In the case of
455 earthquake risk transfer, for instance, each of the earthquake events in the catastrophe risk model needs to be
456 described by its magnitude (if this is the metric of choice for the trigger conditions).

457 **3.1 Choosing the trigger parameters for volcanic eruptions**

458 In our case study, we have researched several physical parameters associated to the phenomenon of volcanic ash falls,
459 as well as Japanese organizations reporting this type of information on a real-time basis while a volcanic eruption
460 unfolds. In Japan, the Japanese Meteorological Agency (JMA) operationally monitors volcanic activity throughout
461 the country and issues relevant warnings and information to mitigate related damages. To continuously monitor
462 volcanic activity, JMA deploys seismographs and related observation instruments in the vicinity of 50 volcanoes that
463 are remarkably active in Japan. When volcanic anomalies are detected, the Agency steps up its monitoring/observation
464 activities and publishes volcanic information and regular bulletins; mainly “Observation Reports on Eruption” and
465 “Volcanic Ash Fall Forecasts” (VAFFs). The Observation Reports and VAFFs are published on a real-time basis for
466 all active volcanoes in Japan; however they contain different types of information. Observation Reports provide
467 information on the ongoing eruption, such as eruption time, eruptive column height (in meters above the crater), the
468 main direction of movement of the eruptive plume at the moment of the report (as per eight cardinal directions: N, E,
469 SE, etc....), and the maximum plume height recorded from the onset of the eruption (Hasegawa et al., 2015). On the
470 other hand, the VAFFs consist of modelled (not observed) ash fall areas and amounts, and are produced when heavy
471 (> 1 mm) or moderate (0.1-1 mm) ash quantities are forecasted in principle. These maps correspond to the moment
472 when the VAFF is issued, and cumulative ash fall map products (i.e. the total accumulated ash fall on the ground
473 throughout the eruption) are not released by JMA.

474 Eruptive column height values are available for each eruptive event present in the volcano risk model. In addition, we
475 estimate the predominant direction of movement of the eruptive plume for each event by assuming it coincides with
476 the main axis of ash fall deposition on the ground. Therefore, we calculate the main direction of deposition of ash fall
477 for each of the event footprints in the model by performing spatial analyses. Resulting azimuths were classified into
478 eight directional sectors (N, NE, E, SE, S, SW, W, and NW) and used as a proxy for the main direction of movement
479 of the generating eruptive ash plume.

480 Based on the above, we selected a combination of two eruption-related parameters (reported eruptive column height
481 and direction of movement of the eruptive plume) for the design of our parametric trigger, since:

- 482 1) These two parameters are reported by JMA on a near-real time basis when an eruption occurs.
- 483 2) The height of the eruptive column and preferential direction of movement of eruptive plume for each of the
484 stochastic events in the model can be assigned based on existing datasets.
- 485 3) We found a significant relationship between eruptive column height and losses as modelled by the volcano
486 risk model (Fig. 3). Pearson correlation tests were performed between eruptive column height and losses, for
487 eight subsets of eruptive events with defined eruptive plume directions (i.e. E, N, NE, NW, S, SE, SW, W).
488 Resulting p-values were all smaller than $\alpha = 0.05$, indicating a significant correlation between eruptive
489 column height and losses for all directional sectors.

490 Other eruption parameters that could be sensitive indicators of losses are total eruption mass and eruption duration;
491 however they were found not to fulfil all the necessary conditions to become part of the trigger design. In the case of
492 total eruption mass, this parameter does not fulfil the requisite of being obtainable on a near-real time basis (condition

493 ~~number 2 in Section 3) - even though it does fulfill conditions 1 and 3 mentioned in the Section. We do not consider~~
494 ~~modelled ash fall areas for the parametric design, given that e~~In particular, cumulative ash fall maps are typically not
495 made typically-available by JMA, and it is thus not straightforward to establish a relationship with losses. Regarding
496 eruption duration, it does not fulfill condition number 3 in Section 3 (this parameter is not part of the stochastic event
497 set in the catastrophe risk model developed). Future development of more complex and complete eruption catastrophe
498 risk models should enable further investigation of alternative parametric designs for volcanic eruptions, using different
499 ~~–or a combination of different- triggers.~~

500

501 **Figure 3: Relationship between height of eruptive column (in ~~k~~Km, from crater rim) and modelled losses for all eruptive**
502 **events in the volcano risk model. Each panel displays a subset of eruptions featuring a specific predominant direction of**
503 **their eruptive plume (East, North, North-East, North-West, South, South-East, South-West and West).**

504

505 3.2 Choosing the trigger type

506 The next step consists of designing the parametric trigger on the basis of the two physical eruptive parameters
507 selected. We have however, several choices in the formulation of such a trigger (Wald & Franco, 2016; Pucciano et
508 al., 2017). In this paper, we focus on two simple variants:

- 509 1) *Binary triggers*, for which each event of the stochastic catalogue can either pay or not pay a fixed monetary
510 amount, P , depending on whether it exceeds the parameter threshold defined by the specific design.
- 511 2) *Multilayer triggers*, for which each event can pay one of N predefined payment levels, associated to a series
512 of defined parameter thresholds.

513 The binary trigger can be seen as a particular case of a multilayer trigger with $N = 1$. As treatment of this case is easier,
514 we start with the design of a binary parametric trigger and we later generalize it to N payment levels.

515 Since we are building a trigger using plume height and ash plume direction expressed as per eight wind sectors (N,
516 NE, E, SE, S, SW, W, NW), it is natural to represent the trigger simply as a set of threshold plume height values for
517 each wind sector, $\{H_s\}_{s \in W}$, where W is the set of the possible wind sectors.

518 This means that if an event i has plume height h_i and wind sector s_i , it triggers a payment if and only if $h_i \geq H_{s=s_i}$,
519 which is the *trigger condition*.

520 We can model the behaviour of the trigger using the stochastic events in the volcano risk model. Let's call T the set
521 of the stochastic events fulfilling the trigger conditions. Since they are the only events releasing a payment, their
522 exceedance rate, collectively, defines the payment occurrence rate.

$$523 \quad R = \sum_{i \in T} r_i$$

524 where r_i stands for the event occurrence rate. From the trigger rate we obtain the yearly triggering probability as $p =$
525 $1 - e^{-R}$ as usual for a Poisson process. The expected payment in a year can be expressed either as $EP = p \cdot P$ or
526 $EP = R \cdot P$ but since we generally have $p \sim R$ the impact of the difference is minimal.

527 If we interpret the trigger as insurance, the EP would correspond to the *pure premium* of the policy, which is a quantity
528 somewhat proportional to its price. Thus, the more often the trigger is activated the more expensive it is. Given a
529 certain trigger payment and a certain yearly budget, we can thus derive a target triggering rate R^* .

530 Since the trigger pays a fixed amount, it will always provide either too much money or too little, if compared to the
 531 actual event loss. This difference is expressed via the following quantity, called **basis risk**, which we define based on
 532 Franco (2010) as:

$$533 \quad BR = BR_+ - BR_- = \sum_{i: l_i < P} (P_i - l'_i) r_i - \sum_{i: l_i > P_i} (l'_i - P_i) r_i$$

534 Where $P_i = P$ if $i \in T$ and 0 otherwise and l'_i represent the loss component in the loss layer of interest. The first
 535 (second) term is called positive (negative) basis risk.

536 3.3 Optimization of the trigger

537 The standard approach to trigger design consists of choosing the trigger thresholds such that basis risk is minimized
 538 (Franco, 2010; Goda, 2013; Goda, 2014; Pucciano et al., 2017). Since the budget and the trigger recovery do tend to
 539 change during the design process, recent approaches have considered the alternative objective that the trigger simply
 540 maximizes the amount of **risk transfer** (Franco et al., 2018; Franco et al., 2019), i.e. find T that maximizes the quantity
 541 defined as:

$$542 \quad K = \sum_{i \in T} r_i l_i$$

543 Where l_i is the loss for event i , that is, we want a trigger which is activated by those events in the catalogue that
 544 collectively have the greater expected annual loss. Maximizing the risk transfer is quite apt, since it states clearly that
 545 the trigger is designed to be activated on the set of events that affect the policy holder the most.

546 Using the trigger condition we can rewrite the risk transfer equation in function of the trigger parameters as

$$547 \quad K(\{H_s\}_{s \in W}) = \sum_{s \in W} \rho_s(H_s) = \sum_{s \in W} \sum_{i: h_i \geq H_s = s_i} r_i l_i \quad (1)$$

548 Where $\rho_s(H_s)$ is the risk transferred by all the events in sector s , which is a function of the threshold value for that
 549 sector, H_s .

550 If we discretize the possible values of H_s in a vector, H_s^k , and we compute all the possible values of rt_s for this vector,
 551 $\rho_s^k = \rho_s(H_s^k)$, we can rewrite the risk transferred per sector as

$$552 \quad \rho_s(H_s) = \sum_k x_s^k \rho_s^k \quad (2)$$

553 Where x_s^k is a vector of 0 and one single 1 placed at the index k' such that $H_s^{k'} = H_s$. This means that we can write
 554 H_s as

$$555 \quad H_s = \sum_k x_s^k H_s^k$$

556 When plugging Eq. (2) in Eq. (1), the risk transfer equation becomes

$$557 \quad K = \sum_{s \in W} \sum_k x_s^k \rho_s^k$$

558 It seems an over complication of a previously simple equation, but actually we eliminated the sum over $i \in T$. Now
 559 the unknown is moved from the set T to the vectors x_s which resembles a problem of linear algebra (it's not, given
 560 the particular form of the vectors, but it's still easier to approach than before). We can now apply similar considerations
 561 to the rate equation obtaining an expression for the payment occurrence rate

$$562 \quad R = \sum_{s \in W} \sum_k x_s^k \lambda_s^k$$

563 where $\lambda_s^k = \sum_{i: h_i \geq H_{s=s_i}^k} r_i$. At this point we can re-write the trigger design as the following optimization problem:

564 find the x_s^k

$$565 \quad \text{which maximize } \sum_{s \in W} \sum_k x_s^k \rho_s^k$$

566 subject to the following constraints:

$$567 \quad \sum_{s \in W} \sum_k x_s^k \lambda_s^k \leq R^*$$

$$568 \quad \sum_k x_s^k H_s^k - \sum_k x_{s'}^k H_{s'}^k \leq \Delta H \quad \forall \text{ adjacent } s, s'$$

$$569 \quad \sum_k x_s^k = 1 \quad \forall s$$

$$570 \quad x_s^k \in \{0, 1\}$$

571 Where R^* is the target trigger rate and ΔH is a maximum threshold difference between two adjacent wind sectors.
 572 Limiting this difference is a way to take into account epistemic risk, that is, risk induced by using a particular model.
 573 It is also a way to decrease trigger sensitivity to the wind sector parameter.

574 The last two constrains, instead, are just a way to express the peculiar form of the x_s vectors.

575 The problem, thus stated, can be solved with linear programming techniques (Franco et al., 2019) or with other
 576 alternative methods (De Armas et al., 2016). The problem is solved in this paper using standard Python libraries for
 577 mixed integer linear programming.

578 As can be seen from the equations for K and R , these two quantities are non-decreasing when the number of trigger
 579 events increases. Thus, maximizing K involves increasing the number of events captured by the trigger (by decreasing
 580 the threshold values) up to a certain point where the critical value R^* is reached. This constraint, as all the other
 581 constraints of the optimization, imposes a trade-off to the $\max(K)$. The curve described by $\max(K)$ in function of R^*
 582 is a Pareto front, an example of which is depicted in Fig. 4.

583

584 **Figure 4: Pareto front for a binary trigger designed modelling stochastic losses for Mt. Fuji. The transferred risk is**
 585 **displayed as percentage of the total risk.**

586

587 In a multi-layer payment trigger, instead of having one single threshold height value we have a series of threshold
 588 values for each wind sector. Each threshold value pays a certain fraction of the maximum payment. Let's suppose we
 589 can generate a two-layer trigger. We decide in advance that the occurrence rate of the first and second payment will
 590 be R_1^* and R_2^* respectively, with $R_1^* > R_2^*$.

591 To build the trigger we follow these steps.

- 592 1) We build a binary trigger, $\{H_s^{(1)}\}_{s \in W}$, with occurrence rate R_1^*
 593 2) We build a second trigger with occurrence rate R_2^* . The problem is identical to the binary one, but with an
 594 additional constraint:

595
$$\sum_k x_s^k H_s^k > H_s^{(1)} \quad \forall s$$

596 Which means that each threshold must be greater or equal to the threshold for that sector in the lower layer. It is easy
 597 to generalise to N layers imposing at each layer n the constraint $H_s^{(n)} > H_s^{(n-1)} \quad \forall s$.

598

599 4 Application and Results

600 For this application, we consider a case where a cedant such as a regional Government may want to consider financing
 601 the risk of economic losses arising from damage to citizens' residential properties in the Prefectures of Tokyo and
 602 Kanagawa, caused by the potential occurrence of damaging eruptive ash fall events. We assume that the Government
 603 has an implicit need to help reconstruct citizens' dwellings after a catastrophic volcanic event, and may therefore want
 604 to consider adopting a parametric risk transfer solution appropriately designed for these cases.

605 The first step consisted of putting together a comprehensive "portfolio" of residential properties for the modelled
 606 geographical area (Tokyo and Kanagawa Prefectures). This portfolio is the input that needs to be provided to the
 607 volcano risk model, for it to calculate potential losses on a probabilistic basis. To do so, we used the census data
 608 incorporated in the model database, which consists of the number of dwellings by administrative unit (Shiku) and by
 609 type of residential occupancy (single family or condominium). The cost of rebuilding each of the properties also needs
 610 to be provided to the model, and we used different information sources to estimate representative rebuilding costs for
 611 single family dwellings and condominiums in the prefectures of Tokyo and Kanagawa (Table 3).

612

613 **Table 3: Representative reconstruction values have been estimated on the basis of several sources of information, including**
 614 **data on building construction values from Japanese Government Statistics (<https://www.e-stat.go.jp>) and insured building**
 615 **values from the General Insurance Rating Organization of Japan (<https://www.giroj.or.jp>).**

616

617 Table 4 provides a summary of the total number of dwellings and corresponding total reconstruction values for the
 618 modelled portfolio.

619

620 **Table 4: Total number of dwellings and total reconstruction values modelled in the volcano risk model for six Japanese**
 621 **volcanoes (by prefecture, and totals). Number of dwellings from Japanese Government Statistics (<https://www.e-stat.go.jp>);**
 622 **Total Values have been calculated on the basis of representative reconstruction values in Table 3.**

623

624 The volcano risk model was run and results were extracted as an “Event Loss Table” or “ELT” (i.e. losses produced
625 by each of the volcanic ash fall events included the model, on the residential portfolio considered). Table 5 provides
626 an example of results for a few ash fall events from Mt. Fuji. Losses can be equal to zero for events either impacting
627 areas outside the model’s geographical domain (i.e. Tokyo and Kanagawa prefectures), or impacting geographical
628 areas within the model domain that have no (modelled) buildings located in them.

629

630 **Table 5: Subset of ELT outputs from the volcano risk model, run of the residential portfolio described. The table shows**
631 **losses on the portfolio caused by four of the model’s ash fall events from Mt. Fuji. The mean loss and the standard**
632 **deviation of the loss distribution associated to each event (in JPY) are reported in the ELT.**

633

634 The ELT results were used to analyse the correlation between height of eruptive column and modelled event losses
635 (Fig. 3), which is a pre-requisite for the selection of this metric for the design of the parametric trigger. Figure 3 plots,
636 for each modelled ash fall event, the height of the eruptive plume (x axis) versus the logarithm of the modelled loss
637 (y axis), showing a strong correlation between the two. Each panel in Fig. 3 depicts eruptive events featuring a specific
638 predominant dispersal direction of their eruptive plume (East, North, North-East, North-West, South, South-East,
639 South-West and West). The correlation between plume height and loss holds for all direction sectors. Dispersion in
640 the plot is due to the fact that the severity of loss, despite being strongly correlated with plume height and plume
641 direction, also depends on other factors, such as duration of the eruption, size distribution of eruptive particles, etc.

642 Calculation of Annual Average Losses (AAL) for the modelled portfolio on a per-volcano basis (Fig. 5, left) shows
643 that Mont Fuji is the main risk source, its average AAL amounting to more than 1 billion JPY per year. Therefore, we
644 chose Mt. Fuji for the calculation of the parametric risk transfer structure. Being located westward of the exposure
645 domain, risk associated to Mt. Fuji is mainly concentrated in the eastern wind sector. In particular, the only sectors
646 containing risk are NE, E, SE, S and SW, even if the last three only in minimal part (Fig. 5, right).

647

648 **Figure 5: (Left) Modelled AAL for the six volcanoes included in the volcano risk model. (Right) Breakdown of Mt Fuji risk**
649 **by wind sector.**

650

651 The occurrence exceeding probability curve (OEP) derived from the modelled losses for Mt. Fuji is depicted in Fig.
652 6. As an example, we imagine that the policy holder might be interested in covering all losses exceeding 30 Billion
653 JPY with a parametric coverage releasing two possible payment levels of 100 and 300 Billion JPY. This means

654
$$l'_i = \min(\max(l_i - 30B, 0), 300B)$$

655 We choose the target exceedance rates for these layers to match the corresponding return period on the OEP curve,
656 3862 and 4944 years. In this way we end up with the trigger OEP curve depicted in Fig. 6.

657 We also imposed a plume height discretization of ~~1k~~km, i.e. $H_s^k = (1\del{k}k\del{m}, 2\del{k}k\del{m}, \dots, 50\text{km})$ and a maximum
658 threshold difference between adjacent sectors $\Delta H = 4\del{k}k\del{m}$.

659

660 **Figure 6: OEP curve for Mt Fuji losses (blue) and trigger payments (orange)**

661

662 The result of the optimization algorithm is depicted in Fig. 7. The (wind sector, plume height) plane is divided into
663 three payment regions, separated by the two trigger layers. As expected, the plume height thresholds are smaller for
664 regions of high risk. The smoothing condition ensures that there is coverage also in the sectors that are adjacent to
665 the sectors at risk, in case that an event has ash fall direction close to the border between two sectors and it is
666 categorized wrongly.

667

668 **Figure 7: Parametric Trigger for Mt. Fuji** Each dashed line correspond to a unit of 10kkm

669

670 Table 6 summarizes the results of the parametric trigger design for the considered cover, including the plume height
671 thresholds by wind sector for the two Layers defined, and the corresponding proportion of risk transferred and layer
672 payments.

673

674 **Table 6: Parametric trigger for Mt Fuji. The risk transferred by each layer is expressed as percentage over the total risk of**
675 **Mt Fuji. The layer payment is expressed as fraction of the maximum payment (300 Billion JPY).**

676

677 The net basis risk of the trigger is 7 Million JPY / year, sum of 32 Million JPY / year of positive and 25 Million JPY
678 / year of negative basis risk, while the expected recovery is of 87 Million JPY / year. The prevalence of basis risk is
679 expected, since the OEP curve of the bond sits on top of the losses OEP in the layer of interest (30 Billion – 330
680 Billion JPY). This amount can be fine-tuned increasing the return periods of the layers until comfortable levels of
681 basis risk are reached.

682 5 Discussion Conclusions

683

684 We present a novel methodology to parameterize financial risk transfer instruments for explosive, tephra fall-
685 producing volcanic eruptions. The design of the parametric product relies on easily obtainable, observable physical
686 parameters relating to explosive volcanic eruptions; namely maximum observed height of the eruptive column and the
687 prevalent direction of dispersal of the associated ash plume.

688 We take as a case study Mount Fuji in Japan, the largest and closest active volcano to the populous Tokyo metropolitan
689 area and the heavily industrialized Kanagawa prefecture (Yamamoto & Nakada, 2015). In Japan, the JMA reports
690 height of the eruptive column and the predominant direction of ash dispersal as part of the “Observation Reports on
691 Eruption” that are released for any erupting volcano on a near-real time basis. The design of the parametric risk transfer
692 for our case study relies on Guy Carpenter’s fully probabilistic model for volcanic eruptions potentially affecting
693 Tokyo and Kanagawa prefectures, which includes 10,000 simulated volcanic ash fall events arising from explosive
694 eruptions of different sizes at Mount Fuji. ~~Therefore, the second pre-requisite for the successful design of an equivalent~~
695 ~~parametric product elsewhere is the existence of a fully probabilistic eruptive loss model encompassing the range of~~
696 ~~all possible eruptive events of interest, and incorporating information relating to plume height and predominant~~
697 ~~direction of ash fall dispersal for each event.~~

698 For the parametric design, we focused on explosive eruptions producing significant tephra loads capable of generating
699 property damages (these are the type of eruptive events considered by the volcano risk model), ~~and took as an example~~

700 a “portfolio” of residential properties representing the existing residential building stock in the Tokyo and Kanagawa
701 prefectures. These could be severely affected by a significant eruption from Mount Fuji- the last Fuji eruption in year
702 1707 is a good example - thus potentially generating a financial burden for the regional and/or or national
703 Governments.

704 We designed a multi-layer trigger assuming that a policy holder might be interested in covering all losses exceeding
705 30 Billion JPY, with a coverage releasing two possible payment levels of 100 and 300 Billion JPY provided the
706 appropriate trigger conditions of eruptive column height and predominant plume direction are met (Table 6). This type
707 of product would provide a policy holder such as a regional Government a quick way to access cash to help repair
708 damages incurred by dwellings as a consequence of a major volcanic eruption, or provide the necessary cash flow to
709 underwriters in these Prefectures (insurance cover for volcanic eruptions is included as part of the standard earthquake
710 policies in Japan).

711 There are several features of the design presented that make it potentially applicable to other volcanic settings where
712 explosive volcanism is typical. In particular, the choice of eruption-related parameters (height of eruptive column and
713 preferential direction of dispersal of ash fall) means that no special monitoring equipment is needed for recordings.
714 Implementation should be straight forward in countries with established volcano observatories, however less than half
715 of the potentially active volcanoes are monitored with ground-based sensors, and even less are considered well-
716 monitored (Brown et al., 2015). This aspect poses a challenge to the global implementation of such product. In this
717 sense, it would be interesting to explore and expand monitoring solutions like satellite-based remote sensing to report
718 both column height and preferential direction of ash fall dispersal on a near real time basis (e.g. Prata et al., 2001;
719 Pardini et al., 2016). An example of such system is HOTVOLC, developed and managed by the Observatoire de
720 Physique du Globe de Clermont-Ferrand (OPGC) and currently operative for 50 volcanoes world-wide (Guéhenneux
721 et al., 2015; <https://hotvolc.opgc.fr>). HOTVOLC reports several eruption-related parameters on a real time basis,
722 including ash plume altitude. On the other hand, it is important that an official, reputable national or regional agency
723 reports such observations in a reliable and timely manner, which could be national volcanological or meteorological
724 agencies, global organizations such as the World Organization of Volcano Observatories (WOVO.org), or perhaps a
725 bespoke global organization akin to Volcanic Ash Advisory Centers (<https://www.icao.int/Pages/default.aspx>).

726 The other important requisite that needs to be in place for the successful design of an equivalent parametric product
727 elsewhere is the availability of a suitable volcano risk model for the area of interest. Such model must be able to
728 generate stochastic loss outputs associated to ash fall-producing eruptions, encompassing the range of all possible
729 eruptive events of interest, and incorporating information relating to plume height and the predominant direction of
730 ash fall dispersal for each event. In an insurance context availability of these models is still rare, since their
731 development requires from a non-negligible investment of time and resources, and volcanic eruptions are generally
732 considered as a “secondary peril” by the insurance industry (e.g. Blong et al., 2017).

733 Further work on the design of volcano-related parametric risk transfer products may relate to different aspects. On one
734 hand, and also considering ash fall-producing volcanic eruptions, the design may be extended to consider other types
735 of damages such as those to crops and livestock, costs arising from ash fall clean up and disposal in urban areas and
736 roads, Business Interruption costs arising from air traffic disruption, airport closures and disruption of critical
737 infrastructures including transportation networks, electricity, water supplies and telecommunications, etc. (Wilson et
738 al., 2012). For any of these types of losses, specific ash fall vulnerability functions must be incorporated in the fully
739 probabilistic volcano model considered. The parametric design presented in this paper could be adapted to coverage
740 of these types of losses, provided a strong correlation was also found between eruptive column height and main
741 direction of ash dispersal and modelled losses.

742 On the other hand, despite ash fall is the volcanic peril with the largest potential of causing wide spread losses (since
743 it is by far the most widely distributed eruptive product), there are other volcanic perils that have a large destructive
744 potential, albeit with a more constrained spatial reach. These include lava flows, pyroclastic density currents, lahars,

745 volcano flank collapses and ballistic blocks (e.g. Loughlin et al., 2015). Design of parametric transfer products for
746 these volcano hazards would entail a rather different approach; concerning both the modelling of losses (starting with
747 the incorporation of these specific hazard events to the fully probabilistic volcano model), to the selection and
748 monitoring of hazard-related trigger parameters.

749
750 The resulting parametric product could be of interest to a number of organizations, including regional and national
751 Governments, but also to economic sectors such as insurers of commercial and industrial properties in these
752 Prefectures (insurance cover for volcanic eruptions is included as part of the standard earthquake policies in Japan).
753 In our case study, we took as an example a “portfolio” of residential properties representing the existing residential
754 building stock in the Tokyo and Kanagawa prefectures. These could be severely affected by a significant eruption
755 from Mount Fuji—the last Fuji eruption in year 1707 is a good example—thus potentially generating a financial burden
756 for the regional and/or national Governments.

757 We designed a multi-layer trigger assuming that a policy holder might be interested in covering all losses exceeding
758 30 Billion JPY, with a coverage releasing two possible payment levels of 100 and 300 Billion JPY provided the
759 appropriate trigger conditions of eruptive column height and predominant plume direction are met (Table 6). This
760 product would provide a policy holder such as a regional Government a quick way to access cash to help repair
761 damages incurred by dwellings as a consequence of a major volcanic eruption.

762 Further work on the design of volcano-related parametric risk transfer products may relate to different aspects. On one
763 hand, and also considering ash fall-producing volcanic eruptions, the design may be extended to consider other types
764 of damages such as those to crops and livestock, costs arising from ash fall clean up and disposal in urban areas and
765 roads, Business Interruption costs arising from air traffic disruption, airport closures and disruption of critical
766 infrastructures including transportation networks, electricity, water supplies and telecommunications, etc. (Wilson et
767 al., 2012). For any of these types of losses, specific ash fall vulnerability functions must be incorporated in the fully
768 probabilistic volcano model considered. The parametric design presented in this paper could be adapted to coverage
769 of these types of losses, provided a strong correlation was also found between eruptive column height and main
770 direction of ash dispersal and modelled losses.

771 On the other hand, despite ash fall is the volcanic peril with the largest potential of causing wide spread losses (since
772 it is by far the most widely distributed eruptive product), there are other volcanic perils that have a large destructive
773 potential, albeit with a more constrained spatial reach. These include lava flows, pyroclastic density currents, lahars,
774 volcano flank collapses and ballistic blocks. Design of parametric transfer products for these volcano hazards would
775 entail a rather different approach; concerning both the modelling of losses (starting with the incorporation of these
776 specific hazard events to the fully probabilistic volcano model), to the selection and monitoring of hazard-related
777 trigger parameters.

778 There are several features of the design presented that make it potentially applicable to other volcanic settings where
779 explosive volcanism is typical. In particular, the choice of eruption-related parameters (height of eruptive column and
780 preferential direction of dispersal of ash fall) means that no special monitoring equipment is needed for recordings.
781 On the other hand, it is important that an official, reputable national or regional agency reports such observations in a
782 reliable and timely manner. Implementation should be straight forward in countries with established volcano
783 observatories. In others, it could be interesting to explore global monitoring solutions like satellite-based remote
784 sensing to report both column height and preferential direction of ash fall dispersal on a near-real-time basis. Such
785 arrangement would provide for a centralised, consistent and independent monitoring solution applicable to explosive
786 eruptions world-wide.

787 ~~The other important requisite that needs to be in place is a suitable volcano risk model that produces stochastic loss~~
788 ~~outputs associated to ash fall producing eruptions. In an insurance context, availability of such models is still rare.~~
789 ~~Nonetheless, increased collaboration between academic experts and the insurance industry brings all the necessary~~
790 ~~elements together for the creation of such models, as it has been in the case presented in this paper. Whereas building~~
791 ~~of volcano loss models requires from a non-negligible investment of time and resources, the availability of open-~~
792 ~~source hazard simulation models such as tephra2 and of global open databases (e.g. wind data, eruptive data, etc.)~~
793 ~~means that the ingredients needed for development are pretty much available on a world-wide basis. Scaling up such~~
794 ~~approach in order to model a significantly larger number of volcanoes than presented in this paper is currently being~~
795 ~~looked into, with promising preliminary results. Increased interest in parametric risk transfer products from the~~
796 ~~insurance industry and capital markets is helping build momentum for the development of risk models of “non-~~
797 ~~traditional” perils such as volcanic eruptions, and the design of associated risk transfer mechanisms.~~

799 6 Conclusions

800 The design of the parametric risk transfer product described in this work displays features, such as its reliance on
801 easily obtainable, observable physical parameters relating to explosive volcanic eruptions, which makes it an attractive
802 option for implementation on a regional or global basis. We believe that global volcano monitoring tools and platforms
803 already in place could be adapted to this end. Notwithstanding the scarcity of fully probabilistic volcano risk models
804 suitable for this purpose, the increased collaboration between academic experts and the insurance industry can bring
805 all the necessary elements together for the creation of such models, as it has been in the case presented in this paper.
806 The availability of open-source hazard simulation models such as tephra2 and of global open databases (e.g. wind
807 data, eruptive data, etc.) means that the ingredients needed for development are pretty much available on a world-wide
808 basis. Scaling up such approach in order to model a significantly larger number of volcanoes than presented in this
809 paper is currently being looked into, with promising preliminary results.

810 These products could be of interest to a number of organizations, including regional and national Governments, but
812 also insurers and other economic sectors. Increased interest in parametric risk transfer products from the insurance
813 industry and capital markets is helping build momentum for the development of risk models of “non- traditional”
814 perils such as volcanic eruptions, and the design of associated risk transfer mechanisms.

827 **References**

828 Artemis (online blog on catastrophe bonds, insurance-linked securities and alternative reinsurance capital). Sompo
829 Japan to launch parametric volcanic risk insurance [Available [http://www.artemis.bm/news/sompo-japan-to-launch-](http://www.artemis.bm/news/sompo-japan-to-launch-parametric-volcanic-risk-insurance/)
830 [parametric-volcanic-risk-insurance/](http://www.artemis.bm/news/sompo-japan-to-launch-parametric-volcanic-risk-insurance/)], 2016.

831 Blong, R.J., Grasso, P., Jenkins, S.F., Magill, C.R., Wilson, T.M., McMullan, K. and Kandlbauer, J.: Estimating
832 building vulnerability to volcanic ash fall for insurance and other purposes. *Journal of Applied Volcanology*, 6:2, 1-
833 13, doi: 10.1186/s13617-017-0054-9, 2017.

834 [Blong R., Tillyard C., Attard G. \(2017\) Insurance and a Volcanic Crisis—A Tale of One \(Big\) Eruption, Two
835 Insurers, and Innumerable Insureds. In: Fearnley C.J., Bird D.K., Haynes K., McGuire W.J., Jolly G. \(eds\)
836 Observing the Volcano World. Advances in Volcanology \(An Official Book Series of the International Association
837 of Volcanology and Chemistry of the Earth’s Interior – IAVCEI, Barcelona, Spain\). Springer, Cham.
838 \[https://doi.org/10.1007/11157_2016_42\]\(https://doi.org/10.1007/11157_2016_42\)
839](https://doi.org/10.1007/11157_2016_42)

840 Bonadonna, C., Costa, A., Folch, A., and Koyaguchi, T.: Tephra dispersal and sedimentation. In: Sigurdsson H,
841 Houghton B, McNutt S, Rymer H, Stix J (eds) *Encyclopedia of volcanoes*, 2nd edn. Elsevier, 587–597, doi:
842 10.1016/B978-0-12-385938-9.00033-X, 2015b.

843 [Brown, S.K.; Loughlin, S.C.; Sparks, R.S.J.; Vye-Brown, C.; Barclay, J.; Calder, E.; Cottrell, E.; Jolly,
844 G.; Komorowski, J.-C.; Mandeville, C.; et al. Global volcanic hazard and risk. In *Global Volcanic Hazards and Risk:*
845 *Cambridge University Press: Cambridge, UK, 2015; pp. 81–172. ISBN 9781316276273*
846](https://doi.org/10.1007/978-3-319-40506-3_17)

847
848
849 Cabinet Office of Japan: Damage estimation of a historic eruption of Mt. Fuji. Cabinet Office of Japan, 124p. (in
850 Japanese), <http://www.bousai.go.jp/kazan/fujisan-kyougikai/report/pdf/houkokusyo7.pdf>, 2002.

851
852 Connor, L.J., Connor, C.B.: Inversion is the key to dispersion: understanding eruption dynamics by inverting tephra
853 fallout. In: Mader, H.M., Coles, S.G., Connor, C.B., Connor, L.J. (eds) *Statistics in volcanology*. IAVCEI
854 Publications, Geological Society of London, 231–242, doi: 10.1144/IAVCEI001.18, 2006.

855
856 Cummins, J.D.: CAT Bonds and Other Risk-Linked Securities: State of the Market and Recent Developments. *Risk*
857 *Management and Insurance Review*, 11, 23-47, doi: 10.1111/j.1540-6296.2008.00127.x, 2008.

858 de Armas J., Calvet L., Franco G., Lopeman M., Juan A.A.: Minimizing Trigger Error in Parametric Earthquake
859 Catastrophe Bonds via Statistical Approaches, in León, R., Muñoz-Torres, M., Moneva, J. (eds) *Modeling and*
860 *Simulation in Engineering, Economics and Management. Lecture Notes in Business Information Processing*,
861 Springer, Cham, 254, 167-175, doi: 10.1007/978-3-319-40506-3_17, 2016.

862 Franco, G.: Minimization of Trigger Error in Cat-in-a-Box Parametric Earthquake Catastrophe Bonds with an
863 Application to Costa Rica. *Earthquake Spectra*, 26 (4), 983-998, doi: 10.1193/1.3479932, 2010.

864 Franco, G.: Construction of customized payment tables for cat-in-a-box earthquake triggers as a basis risk reduction
865 device, in *Proceedings, 11th International Conference on Structural Safety & Reliability*, Taylor & Francis Group,
866 New York, doi: 10.1201/b16387-793, 2013.

867
868 Franco, G.: Earthquake mitigation strategies through insurance, in *Encyclopedia of Earthquake Engineering*, Springer
869 Berlin Heidelberg, 1–18, doi: 10.1007/978-3-642-36197-5_401-1, 2014.

870
871 Franco, G., Guidotti, R., Bayliss, C., Estrada, A., Juan, A. A., Pomonis, A.: Earthquake Financial Protection for
872 Greece: A Parametric Insurance Cover Prototype, in *Proceedings, 2nd International Conference on Natural Hazards*
873 *& Infrastructure*, Chania, Greece, 2019.

874
875 Franco, G., Tirabassi, G., Lopeman, M., Wald, D.J., and Siembieda, W.J.: Increasing earthquake insurance coverage
876 in California via parametric hedges. In Eleventh US National Conference on Earthquake Engineering, 2018.
877
878 General Insurance Association of Japan, Claims associated to weather events.
879 <http://www.sonpo.or.jp/news/statistics/disaster/weather/index.html#2016>, 2015.

880 GVP (Global Volcanism Program), Smithsonian Institution. <https://volcano.si.edu/volcano.cfm?vn=264040>, last access:
881 12 March 2019.

882 Goda, K.: Basis risk for earthquake catastrophe bond trigger using scenario-based versus station intensity-based
883 approaches: A case study for southwestern British Columbia, *Earthquake Spectra*, 29, 757-775, doi:
884 10.1193/1.4000164, 2013.
885
886 Goda, K.: Seismic risk management of insurance portfolio using catastrophe bonds, *Computer-Aided Civil and*
887 *Infrastructure Engineering*, 30, 570–582, doi: 10.1193/1.4000164, 2014.
888
889 Goda K, Franco G, Song J, Radu A (2019): Parametric catastrophe bonds for tsunamis: Cat-in-a-box trigger and
890 intensity-based index trigger methods. *Earthquake Spectra*, 35(1):113–136.

891
892 Government of Japan: Mt. Fuji volcanic disaster prevention measures, [Available at
893 <http://www.bousai.go.jp/kazan/fujisan-kyougikai/report/pdf/houkokusyo7.pdf>], 2004.

894 Guéhenneux, Y.; Gouhier, M.; Labazuy, P. Improved space borne detection of volcanic ash for real-time monitoring
895 using 3-Band method. *J. Volcanol. Geotherm. Res.* 2015, 293, 25–45.
896

897 GVP (Global Volcanism Program), Smithsonian Institution. <https://volcano.si.edu/volcano.cfm?vn=264040>, last
898 access: 12 March 2019.

899 Hasegawa, Y., Sugai, A., Hayashi, Y., Hayashi, Y., Saito, S. and Shimbori, T.: Improvements of volcanic ash fall
900 forecasts issued by the Japan Meteorological Agency. *Journal of Applied Volcanology*, 4 (2), 1-12, doi:
901 10.1186/s13617-014-0018-2, 2015.

902 Jenkins, S., Spence, R., Fonseca, J., Solidum, R., and Wilson, T.: Volcanic risk assessment: Quantifying physical
903 vulnerability in the built environment. *Journal of Volcanology and Geothermal Research*, 276, 105-120, doi:
904 10.1016/j.jvolgeores.2014.03.002, 2014.

905 Jenkins, S., Wilson, T.M., Magill, C.R., Miller, V., Stewart, C., Marzocchi, W. and Boulton, M.: Volcanic ash fall
906 hazard and risk: Technical Background Paper for the UNISDR 2015 Global Assessment Report on Disaster Risk
907 Reduction. Global Volcano Model and IAVCEI. [Available at www.preventionweb.net/english/hyogo/gar], 2015.

908 JMA (Japanese Meteorological Agency): Monitoring of Volcanic Activity.
909 <https://www.jma.go.jp/jma/en/Activities/earthquake.html>, last access: 12 March 2019.

910 Kuge, K., Kawabe, K. and Horie, K.: Proposal for Risk Assessment Method of Volcanic Eruption Damage Estimation
911 of Industrial Facilities against 1707 Hiei Volcano Level (Part 2), Summaries of Technical Papers of Annual Meeting,
912 Architectural Institute of Japan, Structure I, 08, 69-70, 2016.

913 Lloyd’s and Cambridge Centre for Risk Studies. Lloyd’s City Risk Index 2018. [Available
914 at loyds.com/cityriskindex], 2018.

915 Loughlin, S., Sparks, S., Brown, S., Jenkins, S., & Vye-Brown, C. (Eds.). (2015). *Global Volcanic Hazards and Risk.*
916 Cambridge: Cambridge University Press. doi:10.1017/CBO9781316276273

917

918 Macedonio, G. and Costa, A.: Brief Communication "Rain effect on the load of tephra deposits", *Nat. Hazards Earth*
919 *Syst. Sci.*, 12, 1229-1233, doi: 10.5194/nhess-12-1229-2012, 2012.

920 [Magill, C., Mannen, K., Connor, L., Bonadonna, C. and Connor, C., 2015. Simulating a multi-phase tephra fall event:](#)
921 [inversion modelling for the 1707 Hiei eruption of Mount Fuji, Japan. *Bulletin of Volcanology*, 77\(9\), p.81.](#)

922 Maqsood, T., Wehner, M., Ryu, H., Edwards, M., Dale, K. and Miller, V.: GAR15 Regional Vulnerability Functions:
923 Reporting on the UNISDR/GA SE Asian Regional Workshop on Structural Vulnerability Models for the GAR Global
924 Risk Assessment, 11–14 November, 2013, Geoscience Australia, Canberra, Australia, doi:
925 10.11636/Record.2014.038, 2014.

926 Newhall, C. and Self, S.: The Volcanic Explosivity Index (VEI): An Estimate of Explosive Magnitude for Historical
927 Volcanism. *Journal of Geophysical Research*, 87, 1231-1238, doi: 10.1029/JC087iC02p01231, 1982.

928 NOAA/OAR/ESRL PSD: NCEP-DOE Reanalysis 2 data. [Available at <https://www.esrl.noaa.gov/psd/>]

929 Oppenheimer, C.: Climatic, environmental and human consequences of the largest known historic eruption: Tambora
930 volcano (Indonesia) 1815. *Progress in Physical Geography: Earth and Environment*. 27 (2), doi:
931 10.1191/0309133303pp379ra, 230-259, 2003.

932 Oxford Economics: The economic impacts of air travel restrictions due to volcanic ash. Oxford Economics, Oxford.
933 [Available at <https://www.oxfordeconomics.com/my-oxford/projects/129051>], 2010.

934

935 [Pardini, F., Burton, M., Arzilli, F., La Spina, G. and Polacci, M., 2018. SO2 emissions, plume heights and magmatic](#)
936 [processes inferred from satellite data: The 2015 Calbuco eruptions. *Journal of Volcanology and Geothermal Research*,](#)
937 [361, pp.12-24. Merucci, L., Zakšek, K., Carboni, E. and Corradini, S., 2016. Stereoscopic estimation of volcanic ash](#)
938 [cloud-top height from two geostationary satellites. *Remote Sensing*,](#)
939 [8\(3\), p.206.](#)

940

941 [Prata, A.J. and Grant, I.F., 2001. Retrieval of microphysical and morphological properties of volcanic ash plumes](#)
942 [from satellite data: Application to Mt Ruapehu, New Zealand. *Quarterly Journal of the Royal Meteorological Society*,](#)
943 [127\(576\), pp.2153- 2179.](#)

944

945 [Pyle, D.M., 2015. Sizes of volcanic eruptions. In *The encyclopedia of volcanoes* \(pp. 257-264\). Academic Press.](#)
946 [Rougier, J., Sparks, R.S.J., Cashman, K.V. and Brown, S.K., 2018. The global magnitude–frequency relationship for](#)
947 [large explosive volcanic eruptions. *Earth and Planetary Science Letters*, 482, pp.621-629.](#)

948

949 Pucciano, P, Franco, G, Bazzurro, P.: Loss Predictive Power of Strong Motion Networks for Usage in Parametric Risk
950 Transfer: Istanbul as a Case Study. *Earthquake Spectra*, 33-4, 1513-1531, doi: 10.1193/021517EQS032M, 2017.

951

952 Self, S., Rampino, M.R., Newton, M.S. and Wolff, J.A.: Volcanological study of the great Tambora eruption of 1815.
953 *Geology*, 12 (11), 659–663. doi: [10.1130/0091-7613\(1984\)12<659:VSOTGT>2.0.CO;2](https://doi.org/10.1130/0091-7613(1984)12<659:VSOTGT>2.0.CO;2), 1984.

954

955 Spence, R.J.S., Kelman, I., Calogero, E., Toyos, G., Baxter, P.J., Komorowski, J.C.: Modelling expected physical
956 impacts and human casualties from explosive volcanic eruptions. *Natural Hazards and Earth System Sciences*, 5 (6),
957 1003-1015, doi: 10.5194/nhess-5-1003-2005, 2005.

958

959 Stothers, R.B.: The great Tambora eruption in 1815 and its aftermath. *Science*, 224, 1191-1198, doi:
960 10.1126/science.224.4654.1191, 1984.

961

962 Swiss Re: The Fundamentals of Insurance-Linked Securities [Available at [https://www.swissre.com/Library/ils-the-](https://www.swissre.com/Library/ils-the-fundamentals-of-insurance-linked-securities.html)
963 [fundamentals-of-insurance-linked-securities.html](#)], 2011.

964

965
966 [Valade, S.; Ley, A.; Massimetti, F.; D'Hondt, O.; Laiolo, M.; Coppola, D.; Loibl, D.; Hellwich, O.; Walter, T.R.](#)
967 [Towards Global Volcano Monitoring Using Multisensor Sentinel Missions and Artificial Intelligence: The MOUNTS](#)
968 [Monitoring System. Remote Sensing, 2019, 11, 1528.](#)
969
970
971 Wald, D.J., and Franco, G.: Money Matters: Rapid post-earthquake financial decision making, Natural Hazards
972 Observer, Vol. XL, No. 7, October 2016, Natural Hazards Center, University of Colorado, Boulder, [Available at
973 <https://hazards.colorado.edu/article/money-matters-rapid-post-earthquake-financial-decision-making>], 2016.
974
975 Wald, D.J., and Franco, G.: Financial decision-making based on near-real-time earthquake information, in 16th World
976 Conference on Earthquake Engineering, Santiago, Chile, Jan 9th to 11th, 2017, paper #3625, 2017.
977
978 Wilson, T.M., Stewart, C., Sword-Daniels, V., Leonard, G.S., Johnston, D.M., Cole, J.W., Wardman, J., Wilson, G.,
979 and Barnard, S.T.: Volcanic ash impacts on critical infrastructure. Physics and Chemistry of the Earth, Parts A/B/C,
980 45, 5-23, doi: 10.1016/j.pce.2011.06.006, 2012-b.
981
982 World Economic Forum: Convergence of Insurance and Capital Markets. REF: 091008, World Economic Forum,
983 [Available at <https://www.weforum.org/reports/convergence-insurance-and-capital-markets>], 2008.
984
985 Yamamoto, T. and Nakada, S.: Extreme Volcanic Risks 2: Mount Fuji. In: Volcanic Hazards, Risks and Disasters.
986 Editor(s): John F. Shroder, Paolo Papale, Elsevier, doi: 10.1016/B978-0-12-396453-3.00014-9, 2015.
987
988 Yamasato, H., Funasaki, J. and Takagi, Y.: The Japan Meteorological Agency's Volcanic Disaster Mitigation
989 Initiatives. Technical Note of the NIED (National Research Institute for Earth Science and Disaster Prevention), No.
990 380, 101-107, 2013.
991
992
993
994
995
996
997
998
999
1000
1001
1002
1003
1004
1005
1006
1007
1008
1009
1010
1011
1012
1013
1014
1015
1016
1017
1018
1019
1020

1021
1022
1023

Tables

Volcano Name	Number of ash fall events	Aggregate Annual Occurrence Probability
Fuji	9,969	4.84×10^{-3}
Hakone	12,821	6.58×10^{-4}
Asama	832	8.45×10^{-5}
Haruna	651	3.95×10^{-5}
Kita-Yatsugatake	2,065	2.57×10^{-6}
Kusatsu-Shirane	469	6.01×10^{-6}

1024

1025 **Table 1: Number of volcanic ash fall events included in the model (i.e. those ash fall events that impact the model's**
1026 **geographical domain of Tokyo and Kanagawa prefectures) and associated annual probabilities of occurrence by volcano.**
1027 **Ash fall events originated by these volcanoes that do not impact the model domain have been excluded from the counts.**

1028

1029

1030

1031

1032

1033

1034

1035

1036

1037

1038

1039

1040

1041

1042

1043

1044

1045

1046

1047

1048

1049

Function ID	Occupancy	Construction Type	Building Rise	Roof Pitch
1	Resid., Comm. or Indust. Buildings	Wood Frame	Low	Medium
2	Resid., Comm. or Indust. Buildings	Wood Frame	Low	High
3	Resid., Comm. or Indust. Buildings	Wood Frame	Medium	Medium
4	Resid., Comm. or Indust. Buildings	Wood Frame	Medium	High
5	Resid., Comm. or Indust. Buildings	RC-SRC or Steel Frame	Low	Low-Medium
6	Resid., Comm. or Indust. Buildings	RC-SRC or Steel Frame	Low	High
7	Resid., Comm. or Indust. Buildings	RC-SRC or Steel Frame	Medium	Low-Medium
8	Resid., Comm. or Indust. Buildings	RC-SRC or Steel Frame	Medium	High
9	Resid., Comm. or Indust. Buildings	RC-SRC or Steel Frame	High	Low-Medium or High
10	Resid. Buildings	Light Metal Frame	Low	Medium
11	Resid. Buildings	Light Metal Frame	Low	High
12	Resid., Comm. or Indust. Buildings	Light Metal Frame	Medium	Medium
13	Resid., Comm. or Indust. Buildings	Light Metal Frame	Medium	High
14	Resid., Comm. or Indust. Buildings	Light Metal Frame	High	Medium
15	Resid., Comm. or Indust. Buildings	Light Metal Frame	High	High
16	Comm. or Indust. Buildings	Steel Frame or Light Metal Frame	Low	Low-Medium; long-span

1050

1051 **Table 2: Building types common in the Tokyo and Kanagawa Prefectures of Japan, for which specific vulnerability**
1052 **functions were developed in the volcano risk model. RC-SRC stands by “Reinforced Concrete – Steel Reinforced Concrete”.**

1053

1054

1055

1056

1057

1058

1059

1060

1061

1062

1063

1064

1065

1066

1067

1068

1069

1070

1071

1072

1073

1074

1075

1076

1077

1078

Prefecture	Type of Residential Dwelling	Representative reconstruction values (Million JPY)
Tokyo	Single Family	25.5
	Condominium	16.3
Kanagawa	Single Family	22.1
	Condominium	12.3

1079

1080 **Table 3: Representative reconstruction values have been estimated on the basis of several sources of information, including**
1081 **data on building construction values from Japanese Government Statistics (<https://www.e-stat.go.jp>) and insured building**
1082 **values from the General Insurance Rating Organization of Japan (<https://www.giroj.or.jp>).**

1083

1084

1085

1086

1087

1088

1089

1090

1091

1092

1093

1094

1095

1096

1097

1098

1099

1100

1101

1102

1103

1104

1105

1106

	Number of dwellings	Total Value (Million JPY)
Tokyo	6,435,994	121,605,115
Kanagawa	3,828,279	62,788,449
TOTAL	10,264,273	184,393,564

1107

1108 **Table 4: Total number of dwellings and total reconstruction values modelled in the volcano risk model for six Japanese**
1109 **volcanoes (by prefecture, and totals). Number of dwellings from Japanese Government Statistics (<https://www.e-stat.go.jp>);**
1110 **Total Values have been calculated on the basis of representative reconstruction values in Table 3.**

1111
1112
1113
1114
1115
1116
1117
1118
1119
1120
1121
1122
1123
1124
1125
1126
1127
1128
1129
1130
1131
1132
1133
1134
1135
1136
1137
1138
1139
1140
1141
1142
1143
1144
1145
1146
1147
1148
1149
1150
1151
1152
1153
1154

EventID	Volcano	Annual Event Rate	Mean Loss (JPY)	Loss S. Dev. (JPY) (Independent)	Loss S. Dev. (JPY) (Correlated)
1588	Fuji	9.84×10^{-8}	1.03×10^{12}	1.28×10^9	1.32×10^{11}
1589	Fuji	3.65×10^{-7}	1.87×10^6	2.25×10^6	1.93×10^7
1590	Fuji	4.91×10^{-8}	1.36×10^{13}	4.29×10^9	1.01×10^{12}
1591	Fuji	9.82×10^{-7}	0	0	0

1155

1156 **Table 5: Subset of ELT outputs from the volcano risk model, run of the residential portfolio described. The table shows**
 1157 **losses on the portfolio caused by four of the model's ash fall events from Mt. Fuji. The mean loss and the standard**
 1158 **deviation of the loss distribution associated to each event (in JPY) are reported in the ELT.**

1159

1160

1161

1162

1163

1164

1165

1166

1167

1168

1169

1170

1171

1172

1173

1174

1175

1176

1177

1178

1179

1180

1181

1182

1183

1184

1185

1186

1187

1188

1189

1190

1191

1192

1193

1194

1195

1196

1197

1198

1199

1200

1201

1202

1203
1204
1205

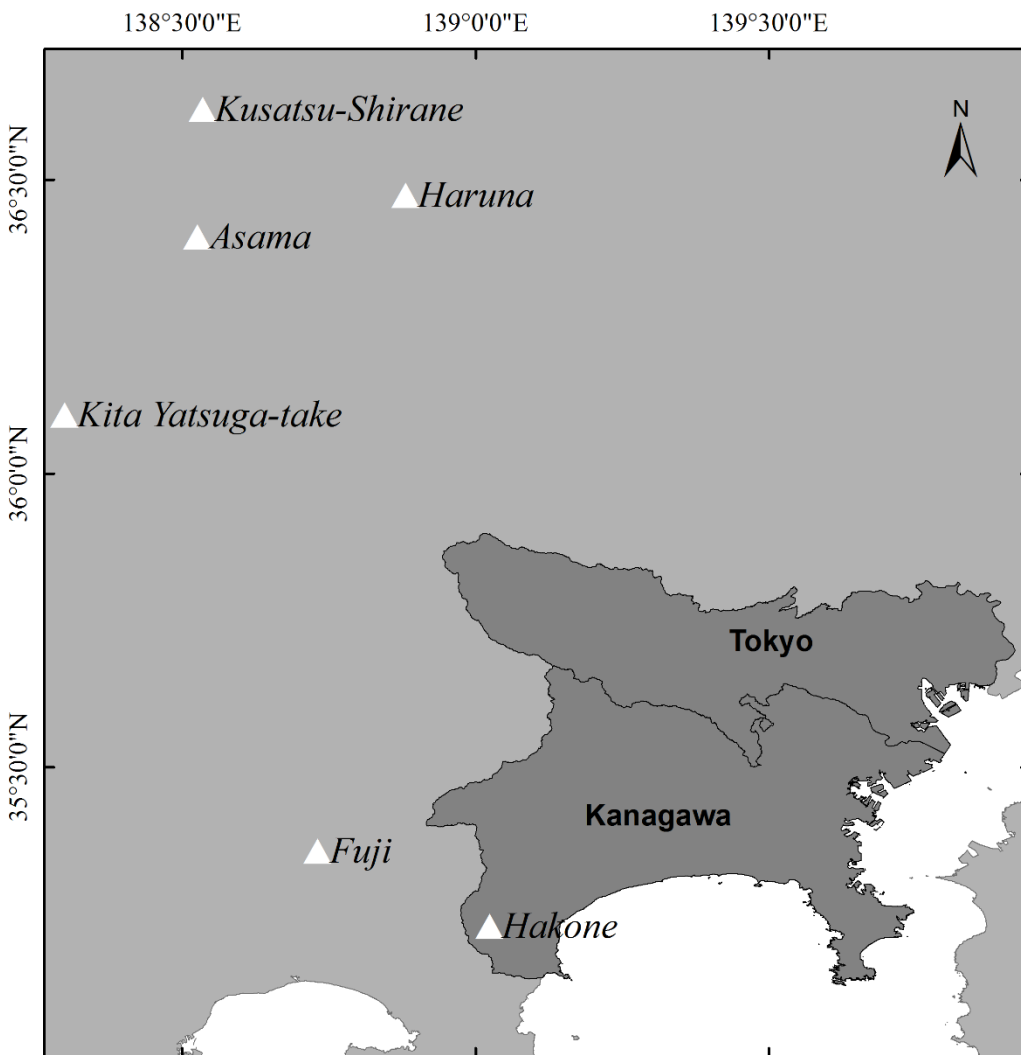
	Plume Height Thresholds [kkm]								Yearly Exceedance Probability	Transferred Risk	Layer Payment
	N	NE	E	SE	S	SW	W	NW			
Layer 1	32	28	28	32	36	37	40	36	0.026%	76%	33%
Layer 2	33	32	29	33	37	40	41	37	0.020%	67%	100%

1206

1207 **Table 6: Parametric trigger for Mt Fuji. The risk transferred by each layer is expressed as percentage over the total risk of**
1208 **Mt Fuji. The layer payment is expressed as fraction of the maximum payment (300 Billion JPY).**

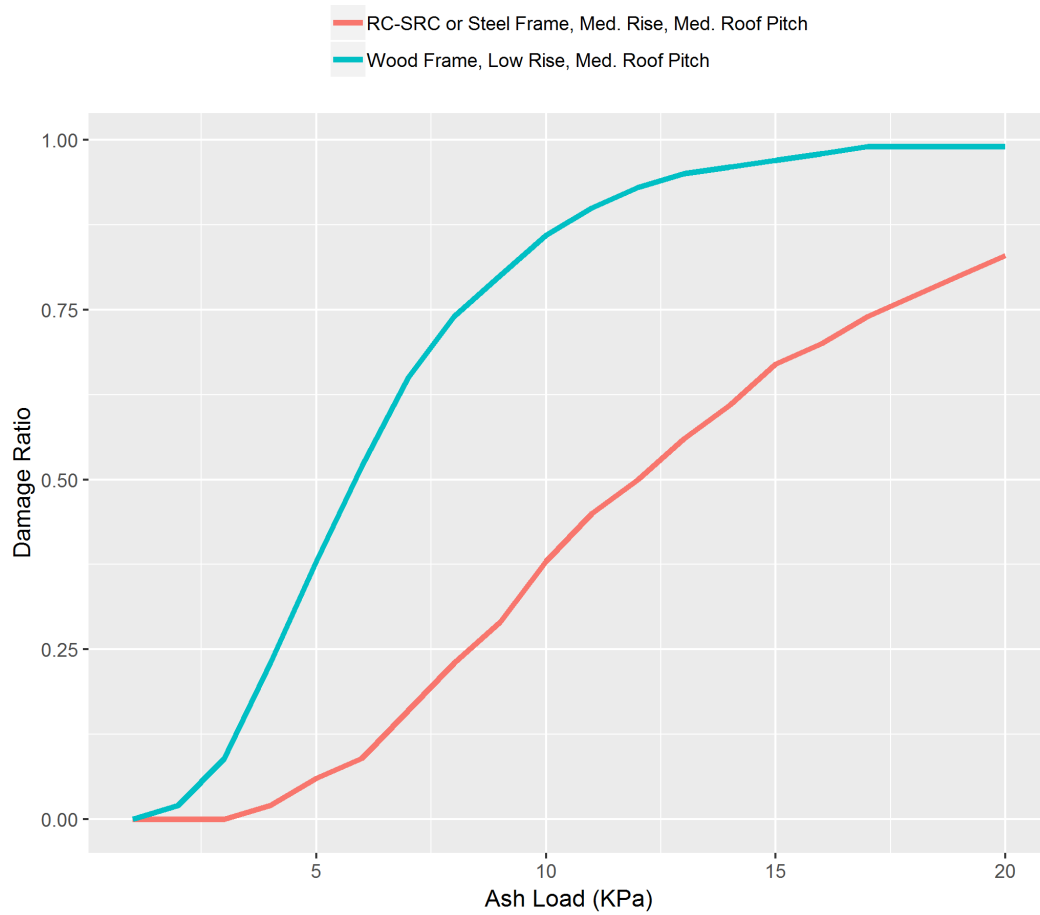
1209
1210
1211
1212
1213
1214
1215
1216
1217
1218
1219
1220
1221
1222
1223
1224
1225
1226
1227
1228
1229
1230
1231
1232
1233
1234
1235
1236
1237
1238
1239
1240
1241
1242
1243
1244
1245
1246
1247
1248

1249 **Figures**
1250
1251
1252



1253
1254 **Figure 1: The geographic domain of the volcano ash fall model presented in this paper includes Tokyo and Kanagawa**
1255 **Prefectures in Japan, and the six major volcanoes that can affect them, Fuji, Hakone, Asama, Haruna, Kita-Yatsugatake,**
1256 **and Kusatsu-Shirane.**

1257
1258
1259
1260
1261
1262
1263
1264
1265
1266

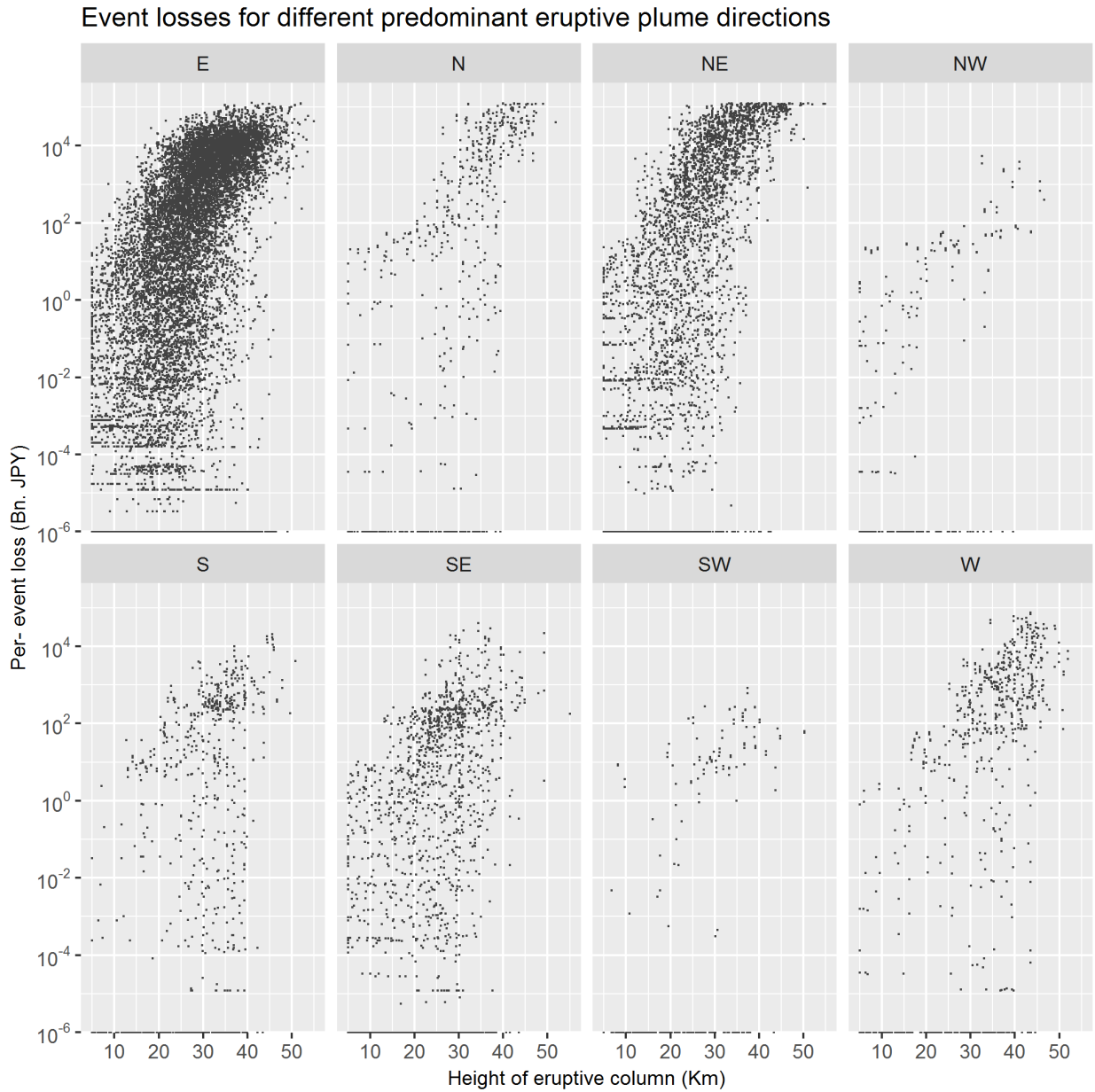


1267
 1268
 1269
 1270
 1271
 1272

Figure 2: Damage functions for two different building types considered in the volcano risk model (“RC-SRC” stands for Reinforced Concrete- Steel Reinforced Concrete; “Med.” stands for Medium); source of these damage functions is Maqsood et al., 2014.

1273
 1274
 1275
 1276
 1277
 1278
 1279
 1280
 1281
 1282
 1283
 1284
 1285
 1286
 1287
 1288
 1289
 1290
 1291

1292
1293
1294
1295

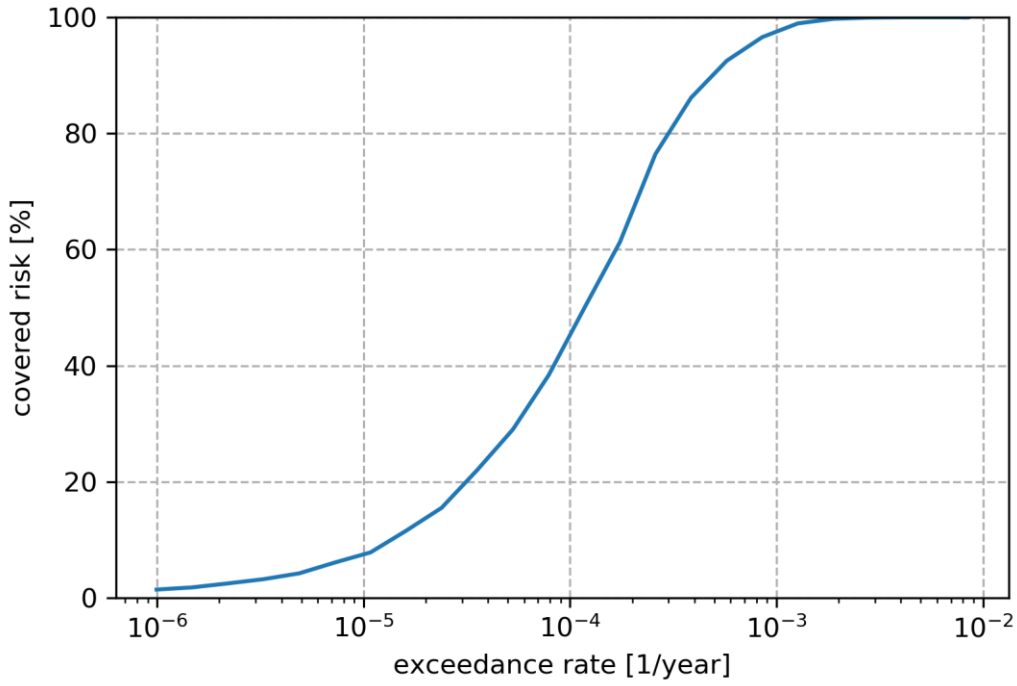


1296

1297 **Figure 3: Relationship between height of eruptive column (in km, from crater rim) and modelled losses for all eruptive**
1298 **events in the volcano risk model. Each panel displays a subset of eruptions featuring a specific predominant direction of**
1299 **their eruptive plume (East, North, North-East, North-West, South, South-East, South-West and West).**

1300
1301
1302
1303
1304
1305

1306
1307

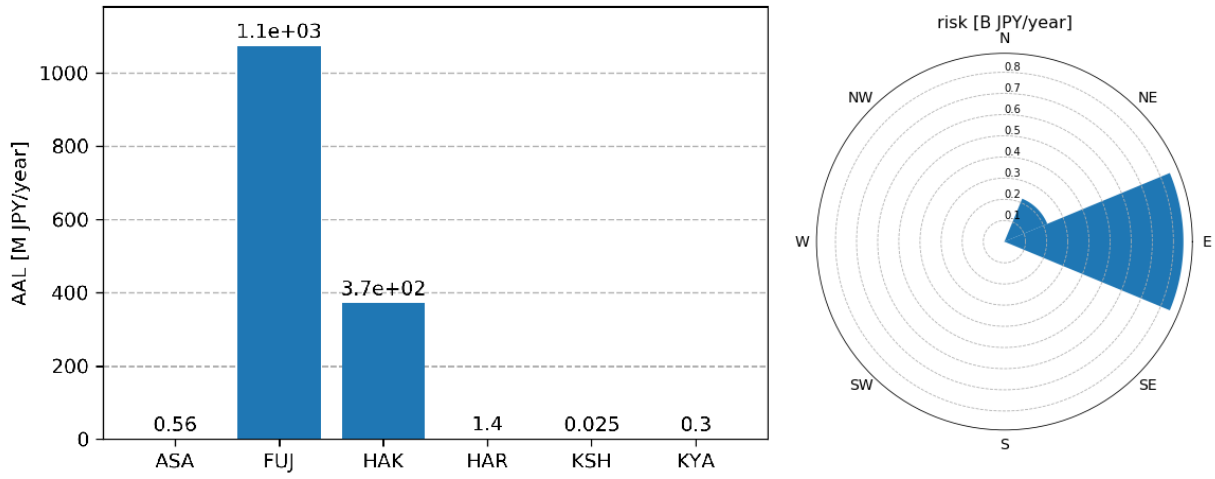


1308
1309
1310
1311

1312 **Figure 4: Pareto front for a binary trigger designed modelling stochastic losses for Mt. Fuji. The transferred risk is**
1313 **displayed as percentage of the total risk.**

1314
1315
1316
1317
1318
1319
1320
1321
1322
1323
1324
1325
1326
1327
1328
1329
1330
1331
1332
1333
1334
1335

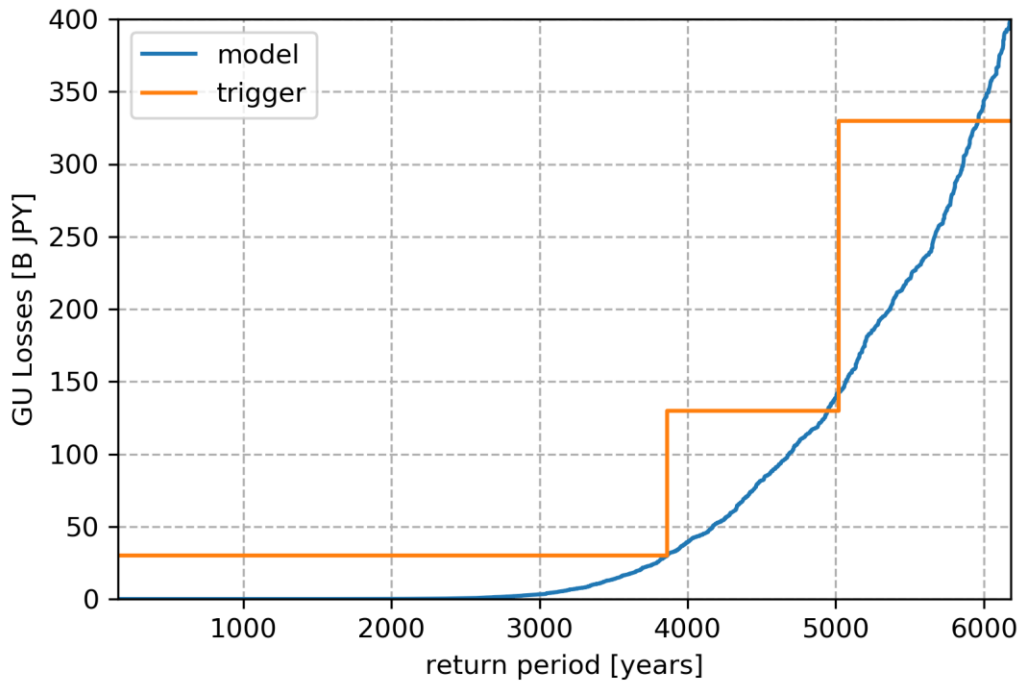
1336
1337
1338



1339
1340
1341
1342
1343
1344

Figure 5: (Left) Modelled AAL for the six volcanoes included in the volcano risk model. (Right) Breakdown of Mt Fuji risk by wind sector.

1345
1346
1347
1348
1349
1350
1351
1352
1353
1354
1355
1356
1357
1358
1359
1360
1361
1362
1363
1364
1365
1366
1367
1368
1369
1370
1371
1372

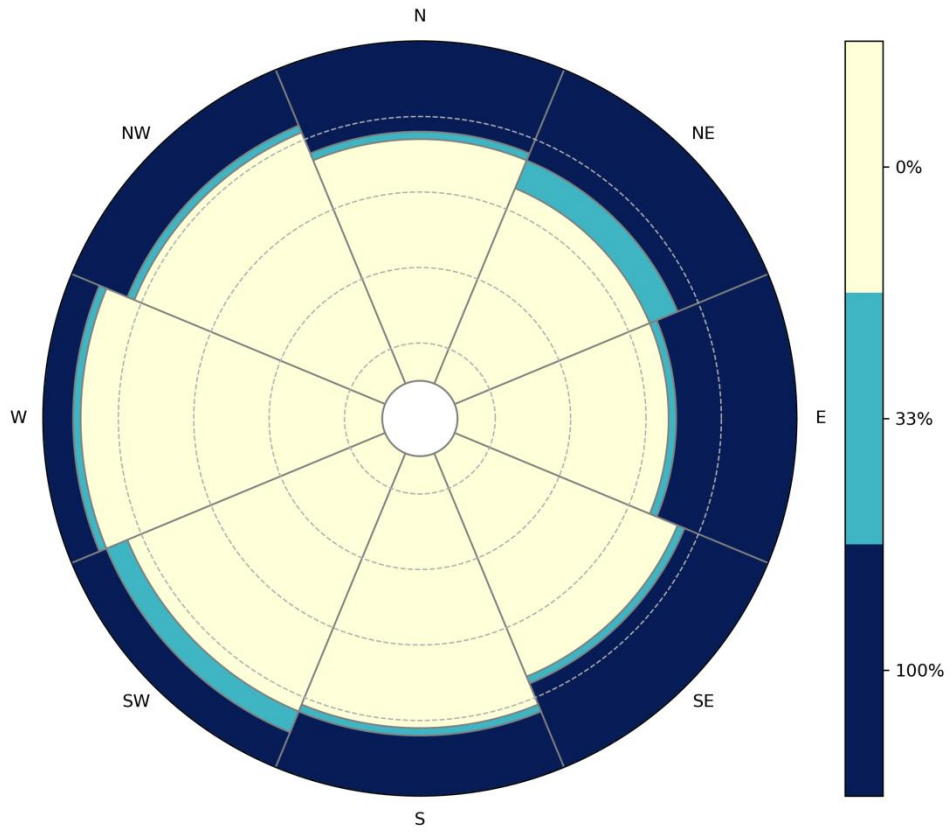


1373
 1374
 1375
 1376

Figure 6: OEP curve for Mt Fuji losses (blue) and trigger payments (orange)

1377
 1378
 1379
 1380
 1381
 1382
 1383
 1384
 1385
 1386
 1387
 1388
 1389
 1390
 1391
 1392
 1393
 1394
 1395
 1396
 1397
 1398
 1399
 1400
 1401
 1402
 1403

1404



1405

1406

Figure 7: Parametric Trigger for Mt. Fuji Each dashed line correspond to a unit of 10 ~~k~~km

1407

1408

1409

1410

1411

1412

1413

1414

1415

1416

1417

1418

1419

1420

1421

1422

1423

1424

1425

1426
1427
1428
1429
1430
1431
1432
1433
1434
1435
1436

1437
1438
1439
1440
1441
1442
1443
1444
1445
1446
1447
1448
1449

1450

1451

1452

1453

Author contribution:

Delioma Oramas-Dorta built the volcano risk model, produced the risk results (“ELT”) associated to the portfolio of residential properties used in the Application, and researched and defined the physical trigger parameters for the design of the volcano risk transfer mechanism presented in the paper. Giulio Tirabassi contributed to the definition of the physical trigger parameters, and coded the mathematical design and optimization of the trigger. Guillermo E. Franco developed the original code as applied to earthquakes, and oversaw the adaptation of the code to the case of volcanic eruptions. Christina Magill produced the tephra fall footprints used in the hazard module of the volcano risk model, while working at Risk Frontiers.

Acknowledgements:

We would like thanking Guy Carpenter for permitting the use of its proprietary Volcano Risk Model for Six Volcanoes in Japan, in order to produce the risk/ loss estimates this study used as a basis to design a parametric risk transfer solution for volcanic eruptions. We would like to acknowledge the providers of several datasets that form part of this Volcano Risk Model. In particular, Risk Frontiers (<https://riskfrontiers.com/>) provided the set of stochastic volcanic tephra fall footprints that are part of the volcano risk model’s hazard module. These footprints were produced in 2017 following commission from Guy Carpenter, to form part of its proprietary Volcano Risk Model for Six Volcanoes in Japan. Development of volcanic tephra fall footprints by Risk Frontiers used wind reanalysis data (NCEP-DOE Reanalysis 2) from NOAA/OAR/ESRL PSD, Boulder, Colorado, USA (<https://www.esrl.noaa.gov/psd/>). Rainfall data that also form part of the model’s hazard module were provided by JBA Risk Management, www.jbarisk.com.